MECHANISMS IN AN ARGON ION PULSED LASER

by

Andrew R. Taylor B.Sc.

A thesis presented to the University of St. Andrews for the Degree of Master of Science, December, 1968.

I hereby declare that this thesis is composed by myself, that it is a record of work carried out by myself, and that it has not been previously presented for a higher degree. The work was carried out in the Physical Laboratories of St. Andrews University under the supervision of A. Maitland.

I certify that Andrew Ramage Taylor B.Sc. has spent four terms as a research student in the Physical Laboratory of the United College of St. Salvator and St. Leonard in the University of St. Andrews, that he has fulfilled the conditions of Ordinance 51 of the University Court of St. Andrews and that he is qualified to submit the accompanying thesis in application for the Degree of Master of Science.

(Supervisor)

CURRICULUM VITAE

In 1962 I was awarded a Russell Residential Scholarship for a four year course leading to a B.Sc. degree in Physics at St. Andrews University. This was completed in June 1966 with First Class Honours and I was then awarded a Carnegie Scholarship to follow a course of research at St. Andrews University. In June 1968 I attended the International Conference of Quantum Electronics held in Miami, Florida and in addition visited several of the laser research establishments on the eastern seaboard of the U.S.A. I am at present completing a ten week course at Dundee Training College for a Teaching Certificate and begin teaching in the new year.

INDEX

CHAPTER I - INTRODUCTION

Although many argon ion lasers, both pulsed and D.C., have been built and used, the mechanisms which cause the required population inversion in the gas are still doubtful, and different views are held by different workers in the field. Many possible mechanisms have been proposed, and the problem of deciding which mechanisms are dominant under given operating conditions, still remains.

The first oscillation in an ion laser was observed by Bell (1) in a pulsed mercury-helium discharge at wavelengths of 6150 Å and 5678 Å, which corresponded to two lines of the Hg II spectrum. There followed observations of laser action in ionised krypton (2), xenon (2) and chlorine (3), as well as many other ions, giving a range of wavelengths extending from the near infrared into the ultraviolet regions of the spectrum. The first observation of oscillation in the ionised argon system was made by Bridges (4) using a pulsed discharge when he observed oscillation on 10 wavelengths in the A II spectrum. The strongest of these were the wavelengths 4880 Å and 5145 Å. Very soon after Gordon et al (5) observed continuous oscillation on 10 wavelengths of the A II spectrum as well as several wavelengths of the Kr II and Xe II spectra. There followed reports on the behaviour of the oscillation in A II under a wide variety of conditions and measurements of the relative gain of the various wavelengths.

Many workers in the argon ion laser field have proposed excitation mechanisms, but the lack of measurements of the fundamental parameters of the system (e.g. electron density, electron temperature etc) have made it difficult to decide which mechanisms are feasible. The problem is that electron densities of the order of 10^{15} cm^{-3} are common with electron temperatures in the region of $10^{4} \rightarrow 10^{5}$°K. Probe measurements in this region are notoriously unreliable, while microwave measurements fail completely. An extension of the microwave technique using optical frequencies, to permit penetration of the plasma at high electron densities, provides an estimate of the parameters involved, and line broadening due to the Stark effect can also be used to determine the charged particle density. Using spectroscopic techniques Kitaeva, Osipov and Sobolev (6) have measured electron densities and electron temperatures in an argon ion laser at a current density of about 400 Acm^{-2}. Measurements from the Doppler broadening of the argon ion spectrum enabled estimates of the ion temperature to be made. There is no information available for current densities of about 5000 Acm^{-2} and pressures of 30 m torr, so extrapolations must be made from the Russian data to give estimates of the parameters to deduce which mechanisms are important. The behaviour of the system can then be predicted and the predictions compared with observation to deduce which mechanism is dominant.

CHAPTER II - INTRODUCTORY LASER THEORY

2.1 Emission and Absorption of Radiation by Atomic Systems.

Atoms, ions and molecules can exist in certain stationary states each having a discrete value of energy. Transitions between these states can occur with simultaneous emission or absorption of radiation, or with the transfer of energy to or from another system. The former type of transition is called a radiative transition, and the frequency of the emitted or absorbed radiation (ν_{nm}) is given by

$$\nu_{nm} = \frac{E_n - E_m}{h} \qquad (2.1.1)$$

where the subscripts n and m refer to the upper and lower energy states respectively, E_n is the energy of state n, and h is Planck's constant. Several types of radiative transition are possible. An atom in a high energy state can transfer to a lower energy state without any external influence by spontaneous emission, where the transition is accompanied by the emission of an energy quantum, and no definite phase or direction correlations exist between successive spontaneous emission quanta. The probability of transition per sec between two states n and m is denoted A_{nm}. The atom can also decay to a lower energy state by stimulation with an electromagnetic field of the appropriate frequency ν_{nm}, and in this process the stimulated quantum has the same phase and direction as the quantum causing stimulation. The stimulated emission probability between two states n and m will be proportional to the radiation density (u)

at the frequency ν_{nm} with the constant of proportionality denoted B_{nm}, so that the total probability per sec of an emission process is

$$P_{nm} = A_{nm} + uB_{nm} \qquad (2.1.2)$$

An atom in state m can absorb a quantum and become excited into a higher energy state (n), provided the quantum has the frequency ν_{nm} satisfying equation (2.1.1). This process is again proportional to the radiation density at frequency ν_{nm} so the total probability of an absorption process is denoted by

$$P_{mn} = uB_{mn} \qquad (2.1.3)$$

The quantities A_{nm}, B_{nm} and B_{mn} are called the Einstein coefficients and are constant for a given transition. It can be shown that they are related (7) by

$$g_n B_{nm} = g_m B_{mn} \qquad A_{nm} = \frac{8\pi h\nu^3}{c^3} B_{nm} \qquad (2.1.4)$$

where c is the velocity of light in vacuo and g_n denotes the degeneracy of the level n (i.e. the number of states of the atom which have the same energy E_n).

2.2 Lifetimes and Linewidths.

The total probability per sec for the decay of an atom in state n to any other state of the system can be expressed as a sum of the partial decay probabilities per sec between state n and state i of

the system viz.

$$A_n = \sum_{i=1}^{n-1} A_{ni} \qquad (2.2.1)$$

Clearly, instead of giving the total transition probability per sec we could define a characteristic time τ_n, in which the population of state n would decrease to a value $\frac{1}{e}$ of its value at t = o, then these two quantities A_n and τ_n would be simply related by

$$A_n = \frac{1}{\tau_n} \qquad (2.2.2)$$

The effective radiative lifetime (τ_{nm}) of the radiation emitted spontaneously between levels n and m can be related to the lifetimes of levels n and m (8) by

$$\frac{1}{\tau_{nm}} = \frac{1}{\tau_n} + \frac{1}{\tau_m} \qquad (2.2.3)$$

and the probability dP of radiating a wave train of time duration t is given by

$$dP = \frac{1}{\tau_{nm}} \exp[-\frac{t}{\tau_{nm}}] \, dt \qquad (2.2.4)$$

This 'interrupted' type of radiation (i.e. a wave of frequency ν_{nm} lasting for time t) is equivalent to a summation of waves with a frequency spread about the centre frequency ν_{nm}. The shape of the intensity distribution $a(\nu)$ is obtained from the Fourier analysis of equation (2.2.4), and is a Lorentzian distribution with form (9)

$$a(\nu) \propto \frac{1}{(\nu-\nu_{nm})^2 + \Delta\nu_N^2} \qquad (2.2.5)$$

where $\Delta\nu_N$ is the half width of the distribution (i.e. the width at the half power points) and is the natural line width for an isolated radiating atom.

In general the atoms will be moving with a velocity component v relative to the observer, who will measure frequency $\nu_{nm}(1 + \frac{v}{c})$ as a consequence. This will cause another type of broadening called Doppler broadening which has a distribution described by

$$a(\nu) \propto \exp[-\frac{(\nu-\nu_o)^2 \ell n2}{\Delta\nu_D}] \qquad (2.2.6)$$

where $\Delta\nu_D$ is the half width of the Doppler profile and is given by

$$\Delta\nu_D = \nu_o \frac{2KT}{Mc^2} \ell n2 \qquad (2.2.7)$$

where K = Boltzmann's constant

T = absolute temperature of atoms

M = mass of atom

ν_o = central frequency of distribution.

Another broadening mechanism is the effect of collisions on the emission. This process is equivalent to interruption of the emitting atom giving a Lorentzian profile, as for the natural broadening. The half-width is denoted $\Delta\nu_L$. For this effect to broaden the line, the time between collisions must be less than the time for the emission of the radiation.

It is usual to split broadening into two types - homogeneous and inhomogeneous. In the former all the emitting atoms contribute to a point on the intensity distribution and we cannot associate any particular group of atoms with any particular frequency (e.g. Lorentzian broadening). In the latter, each atom emits homogeneously, but the centre frequencies are different for different atoms, so that the envelope of all the homogeneous distributions gives an inhomogeneous distribution (e.g. Doppler broadening). In this type we can associate a definite population with any frequency interval on the distribution.

In general the emission or absorption frequency distributions are a mixture of Lorentzian and Doppler broadening, and only under certain conditions do one or other of the types dominate. In particular in an argon ion laser the linewidth of the medium is predominantly Doppler broadened with a linewidth of about 1000 Mc/s. The natural linewidth is about 75 Mc/s.

2.3 Gain.

When radiation of constant intensity I_o but variable frequency ν is incident upon a medium, then at depth x into the medium can be expressed in terms of an absorption coefficient K_ν by

$$I_\nu(x) = I_o e^{-K_\nu x} \qquad (2.3.1)$$

Consider a parallel beam of light with frequency between ν and

$\nu + d\nu$ travelling between planes x and $x + dx$ with a velocity $v = \frac{c}{\eta}$, where η is the refractive index of the medium and c is the velocity of light in vacuo. If $dN_{n\nu}$ atoms cm^{-3} in level n are capable of emitting in the frequency range ν and $\nu + d\nu$, and $dN_{m\nu}$ atoms cm^{-3} in level m are capable of absorbing in the same frequency range, then the decrease of energy of the beam in distance $x \to x + dx$ is just the difference in absorption and emission of radiation between levels n and m, given by

$$-d(I_\nu d\nu) = h\nu[B_{mn}\, dN_{m\nu} - B_{nm}\, dN_{n\nu}]I_\nu \frac{dx}{v} \qquad (2.3.2)$$

The spontaneous emission will not contribute significantly to the beam as it is not emitted coherently (i.e. with same phase and direction as the incident beam). It will contribute a small part detectable as noise in the system. Rearranging (2.3.2) gives

$$-\frac{1}{I_\nu}\frac{dI_\nu}{dx}\, d\nu = \frac{h\nu\eta}{c}[B_{mn}\, dN_{m\nu} - B_{nm}\, dN_{n\nu}] \qquad (2.3.3)$$

Integrating (2.3.3) over the entire line centred on ν_{nm} and substituting K_ν from (2.3.1) gives

$$\int K_\nu\, d\nu = \frac{h\nu_{nm}\eta}{c}[B_{mn}\, N_m - B_{nm}\, N_n] \qquad (2.3.4)$$

Using Einstein's relations (2.1.4) in (2.3.4) gives the total absorption from the incident beam as

$$\int K_\nu\, d\nu = K'[N_m - \frac{g_m}{g_n} N_n] \qquad (2.3.5)$$

where $K' = \frac{c^2 A_{nm} g_n}{8\pi\nu_{nm}^2 \eta^2 g_m}$ is a constant for a given pair of levels n and m. Formula (2.3.5) is the Füchtbauer-Ladenburg formula (10). It can be seen from this that in order to achieve gain in the medium, then K_ν must be negative to give negative absorption or gain. This implies that a necessary condition for gain is that

$$\frac{N_n}{g_n} > \frac{N_m}{g_m} \qquad (2.3.6)$$

This condition can be satisfied for specific transitions in certain materials by exciting the atoms into the upper energy levels in some way (e.g. by supplying energy from an electrical discharge in a gas). In an argon ion laser the lifetime of the lower laser states is $\sim$ 1 nsec and this means that ions arriving in this state quickly decay into the ground state, so that the population of the lower level is small. The mechanisms exciting the ions ensure that a large population exists in the upper laser state so that equation (2.3.6) is satisfied. This provides a means of obtaining gain in a system.

2.4 Cavity Modes

If the amplifying medium is to be used to produce oscillations, there must be feedback into the system. To do this the amplifying

medium is introduced into a resonant cavity formed by two highly reflecting mirrors (typically $\sim 95 \rightarrow 100\%$ reflecting). A large fraction of the power is fed back into the medium and traverses the cavity many times. However only certain frequencies will satisfy the phase conditions imposed on the radiation in the cavity by the boundary mirrors. Standing waves will be set up if, after two transits of the cavity length (d), the wave returns with the same phase as before (i.e. if the distance travelled equals an integral number of wavelengths λ_m). The permitted wavelengths must satisfy

$$2d = m\lambda_m \qquad (2.4.1)$$

where the integer m defines the mth longitudinal mode of the cavity. Transverse modes are also possible and will depend on the diffraction losses caused by the mirrors defining the cavity (11).

The frequency separation of the longitudinal modes can be found using the relation between the wavelength and frequency (ν_m) of the mth longitudinal mode

$$\nu_m = \frac{c}{\eta\lambda_m} \qquad (2.4.2)$$

where η = refractive index of medium.

The frequency separation of adjacent modes is thus

$$\Delta\nu = \nu_{m+1} - \nu_m = \left(\frac{c}{2d\eta}\right)(m+1) - \left(\frac{c}{2d\eta}\right)m = \frac{c}{2d\eta} \qquad (2.4.3)$$

If the gain profile of the amplifying medium is broader than $\Delta\nu$ then several modes will be able to have gain in the medium and will oscillate when this gain is greater than the losses for that mode. The reflection losses occurring at the mirrors are the same for each mode, but diffraction losses at the mirrors will depend on the field pattern of the mode and the mirror shape. The steady state field distribution in cavities of different geometries have been calculated by two different methods. Fox and Li (12) started with a plane wave at one mirror and using Huygen's principle calculated the field distribution at the other mirror. Using the new field distribution they repeated this several hundred times with a computer until a stable configuration was achieved. This configuration was then a stable solution for an allowed mode pattern. Boyd and Gordon (13) used the fact that the field distribution at one mirror caused by that distribution at the other mirror must reproduce itself within a constant factor in its spatial variation, for stability. Substitution in Huygen's principle would then give stable solutions for the particular geometry chosen.

2.5 Hole burning effects.

The term hole burning is used to describe the selective depletion of the population of gas atoms (e.g. depletion of only those atoms with velocities in a selected range). The radiative

lifetime of the stimulated emission must be short compared with the energy exchange processes for this effect to be produced (i.e. the line is inhomogeneously broadened). The gain profile of an inhomogeneously broadened line can be represented as shown in fig. 2.1. The cavity longitudinal modes occur at the vertical bars so that oscillation is possible if the gain is greater than the losses for one of these modes. The losses can be represented by a horizontal line as shown, and the modes (a), (b) and (c) will oscillate. This will 'burn out' the population within the homogeneous line profile about the cavity mode. The population in the cross hatched area is depleted by this oscillation. Providing that the homogeneous line width is less than the spacing of the cavity modes, the atoms contributing to the gain in one mode cannot couple to those of another mode, but, if the mode spacing becomes comparable with the homogeneous line width, the holes overlap and coupling is possible. It can be shown (14) that the condition for overlapping of holes is that

$$\frac{c}{2d} = (1 + \frac{I}{I_o})^{\frac{1}{2}} \Delta\nu_N \qquad (2.5.1)$$

where c = velocity of light; I = radiation intensity; d = laser length; I_o = radiation intensity at threshold; $\Delta\nu_N$ = natural line width

Typical values for $\frac{I}{I_o} = 9$ and $\Delta\nu_N = 75$ Mc/s will give overlapping of holes for a laser > 70 cms long.

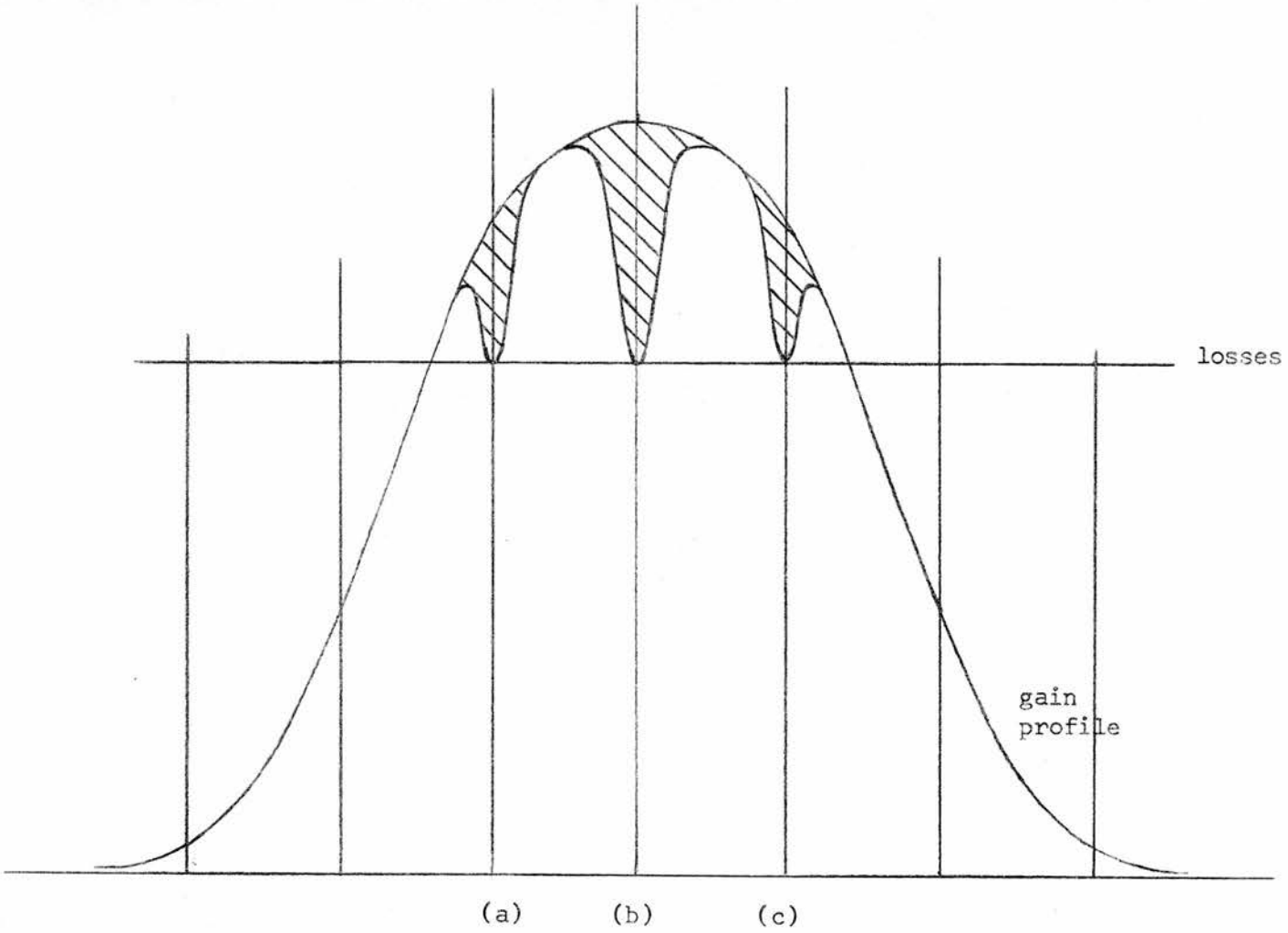

Fig. 2.1: 'Hole burning' in an inhomogeneously broadened system.

2.6 Gain Saturation.

Whenever the condition that the gain exceeds the losses is satisfied for a particular frequency, the stimulated emission intensity would increase exponentially with time, but in practice the laser settles to a steady state intensity and is said to be saturated. The onset of oscillation causes the inverted population to be reduced and this in turn reduces the gain, until a steady state is reached. The effect of gain saturation is dependent on the type of line broadening in the system, and it can be shown (15) that for inhomogeneous broadening the gain (g) can be written

$$g = g_o\left(1 + \frac{I}{I_o}\right)^{-\frac{1}{2}} \qquad (2.6.1)$$

where I = radiation field intensity

I_o = function of the Einstein coefficients and transition probabilities for a given transition

g_o = gain when $I \equiv 0$

Two factors become important in considering the stimulated emission oscillations, one of which is the threshold (i.e. when does the gain become greater than the losses). This will determine which of several lines oscillate first. The other factor is the gain saturation, which will determine the final intensity of the emission once the first condition is satisfied. These factors become important when considering the behaviour of oscillations having

common upper or lower levels. It will be seen how these two factors determine the order and intensity of the stimulated emission at various wavelengths in the system to be studied. These results are presented in Chapter VI.

CHAPTER III - GAS LASERS

3.1 Introduction

It is useful to compare the mechanisms of other gas lasers with those of the argon ion gas laser. The level scheme is first generalised and then each type of gas laser is discussed in terms of a common example of the type.

Gas lasers can be divided arbitrarily into 3 groups viz. neutral atom, ion and molecular. We shall refer to the atoms, ions or molecules as 'particles'. The distribution of energy levels of a particle can be shown in a simplified way in fig. 3.1. The essentials of the scheme are

1) a ground state or long lived metastable state located at zero energy on fig. 3.1
2) a gap E_o to the next higher state, followed by 2 or 3 similar gaps of the same order of magnitude to a few more energy states
3) a large number of levels spaced closely together following the first few levels
4) an ionisation or dissociation energy E_i.

All the states have a certain parity either zero or one and all transitions between states of opposite parity are allowed on a dipole electrostatic approximation.

Direct excitation of any one of the many levels near E_i is small in general, so none are able to achieve a population inversion

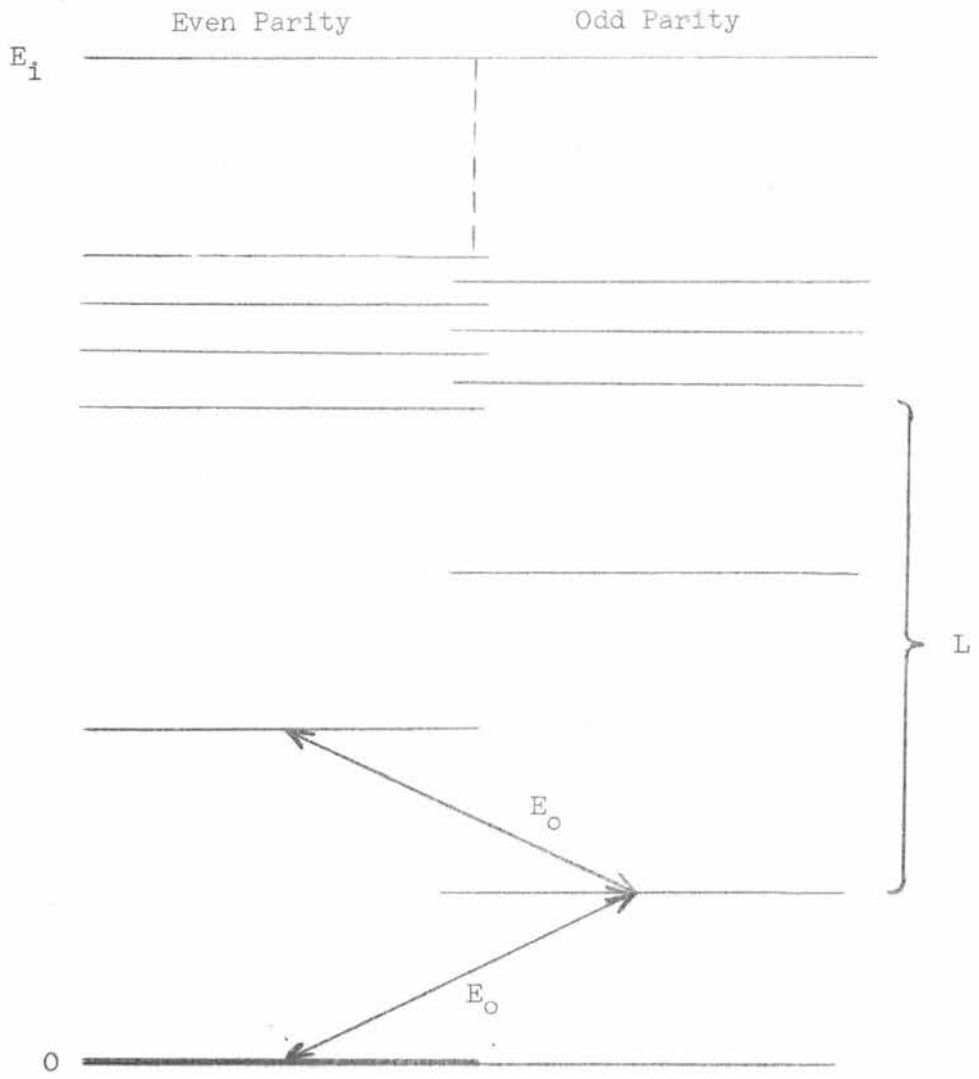

FIG. 3.1 : Simplified energy level diagram for gas lasers.

relative to other levels, sufficient for laser action. Also, levels are so close together that collisional processes thermalise the population distribution despite any selective excitation. Therefore laser action takes place between the levels in region L of the energy diagram.

For neutral atoms $E_i \sim 5 \rightarrow 15$eV and $E_o \sim 0.1 \rightarrow 1$eV giving oscillating wavelengths in range $1 \rightarrow 10$ microns. One important exception is Ne which has very high E_i, and the excitation is a specialised case of excitation transfer by collision of neon ground state atoms with metastable He atoms. For ions, $E_i \sim 12 \rightarrow 25$eV and $E_o \sim 2 \rightarrow 5$eV resulting in oscillation in the visible range. The molecular gas lasers have low $E_i \sim 2 \rightarrow 3$eV and $E_o \sim 0.25$eV so that they generally have transitions giving rise to wavelengths in region $10 \rightarrow 100$ microns. Their level schemes are of course very much more complicated than indicated.

3.2 The Mechanisms of the He-Ne gas laser.

The dominant excitation mechanism in a He-Ne laser is a resonant transfer by collisions of the second type i.e. collisions of the type

$$A^* + B \rightarrow A + B^*$$

where the asterisk denotes an excited atom.

The He atom is excited into the $^3S_1$ or $^1S_0$ states by collision with energetic electrons and then, in a collision of the second kind, resonant transfer of energy into the 3s and 2s states of the Ne atom occur. These decay by stimulated emission to the 3p and 2p levels producing three main laser lines viz. 3.39 microns [3s → 3p], 6328 Å [3s → 2p] and 1.15 microns [2s → 2p]. A simplified diagram of the processes involved is shown in fig. 3.2. The spontaneous emission transitions and the other levels have been omitted for simplicity.

The decay of the 1s state is by collision or spontaneous radiation to the ground state. The density of atoms in the ground state is high and conditions for radiation trapping can exist, thus effectively increasing the lifetime of the 1s transition from about 1 nsec to 1 μsec. The dominant decay is then by collisions with atoms or the tube walls. The population in the 1s states builds up and causes a similar 'bottleneck' on the 2p states, which will cause saturation of the stimulated emission output. The 1s states can also be excited by inelastic electron collision with ground state atoms, and the metastable He states can be deexcited by electron collision, both processes leading to saturation of the stimulated emission. Bennett (16) holds the view that saturation is caused by either electron collision excitation from the 1s states or by resonance trapping in the 1s → 2p transitions. The observed excitation dependence of the

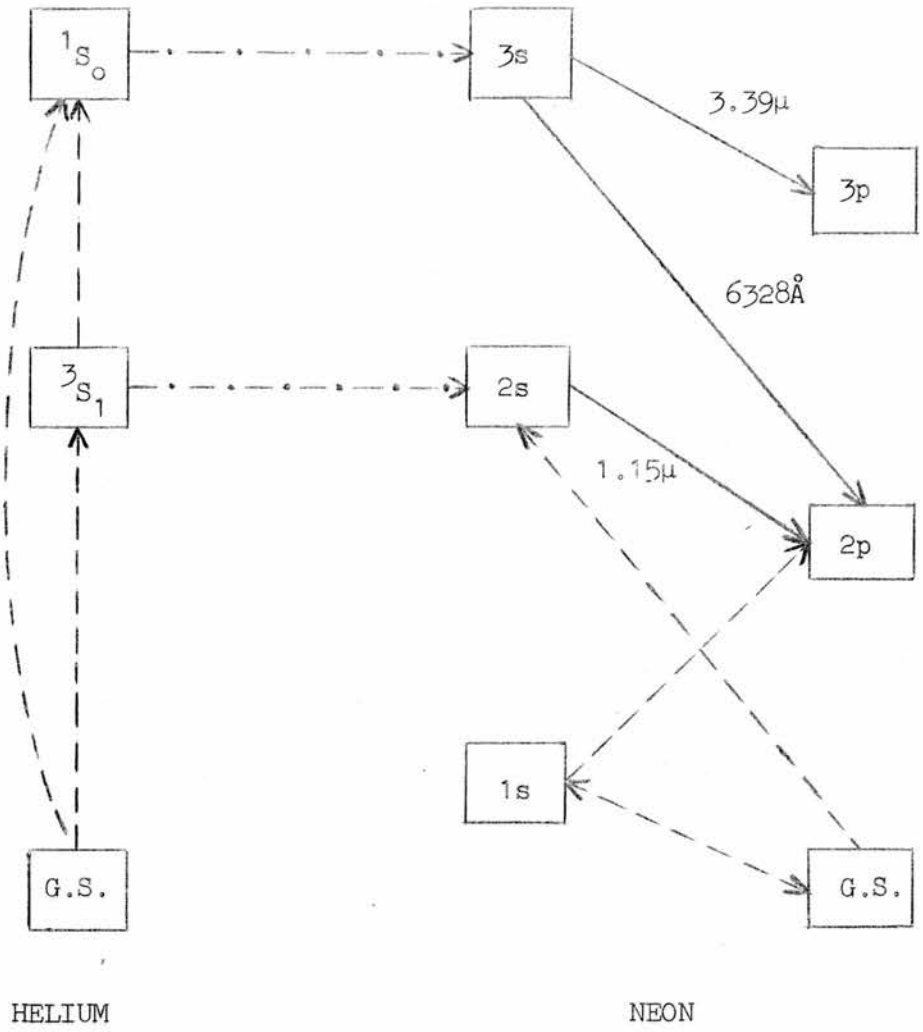

FIG. 3.2 : Simplified energy level diagram for the He-Ne gas laser.

radial dependence of gain suggests radiation trapping as the dominant effect. White and Gordon (17) put forward the view that the saturation is caused by levelling out of the density of the metastable helium atoms. They base this view on measurements of the dependence of the $^1S_0$ metastable density with current mode with both spectroscopic and microwave methods.

It has been suggested that resonance trapping is a possible mechanism for increasing the lifetimes of the 4s ion states in argon, which are the lower levels for stimulated emission, so this effect is dealt with in more detail in section 4.5 and evidence for this effect presented in section 7.5.

3.3 The mechanisms of the CO_2 - N_2 laser.

In lasers which use atomic electronic energy levels to provide laser action, the energy levels lie well above the ground state of the atom. Typically the upper and lower laser transition levels are about 14eV above the ground state and have a spacing of about 1.5eV. This means that it requires an excitation energy of 14eV to provide a stimulated photon of energy 1.5eV so that, assuming all excitations into the upper laser level provide a stimulated photon, the maximum possible efficiency for energy conversion is about 10%. This is the quantum efficiency of the transition involved. In order to attain an efficiency of

this order it is necessary to selectively excite the upper laser levels and this is sometimes not possible, so that in an atomic laser of quantum efficiency 10% a typical practical efficiency would be about 0.01%. In the CO_2 - N_2 gas laser however, with a quantum efficiency of about 40%, it is possible to achieve practical efficiencies of about 30% by selective pumping of the upper laser levels.

The carbon dioxide molecule has 3 possible vibrational modes (18) viz. the symmetric stretch mode, the bending mode and the asymmetric stretch mode. The energies of these 3 modes are quantised and denoted by quantum numbers so that CO_2(201) represents a CO_2 molecule with 2 quanta of energy in the symmetric stretch mode, zero quanta in the bending mode and one quantum in the asymmetric stretch mode. Each vibrational level is split into several rotational modes, and transitions occur between two different rotational states belonging to two different vibrational levels. In the CO_2 laser the main transitions have an (001) upper level and (100) and (020) lower levels corresponding to wavelengths 10.6 and 9.6 microns respectively (See fig. 3.3). The excitation into the upper laser state is by electron collision which preferentially excites the (00n) states. Collision of the excited molecules in the (00n) states, with unexcited CO_2(000) molecules causes efficient transfer of 1 quantum of energy, since the vibrational (00n) levels are nearly equally

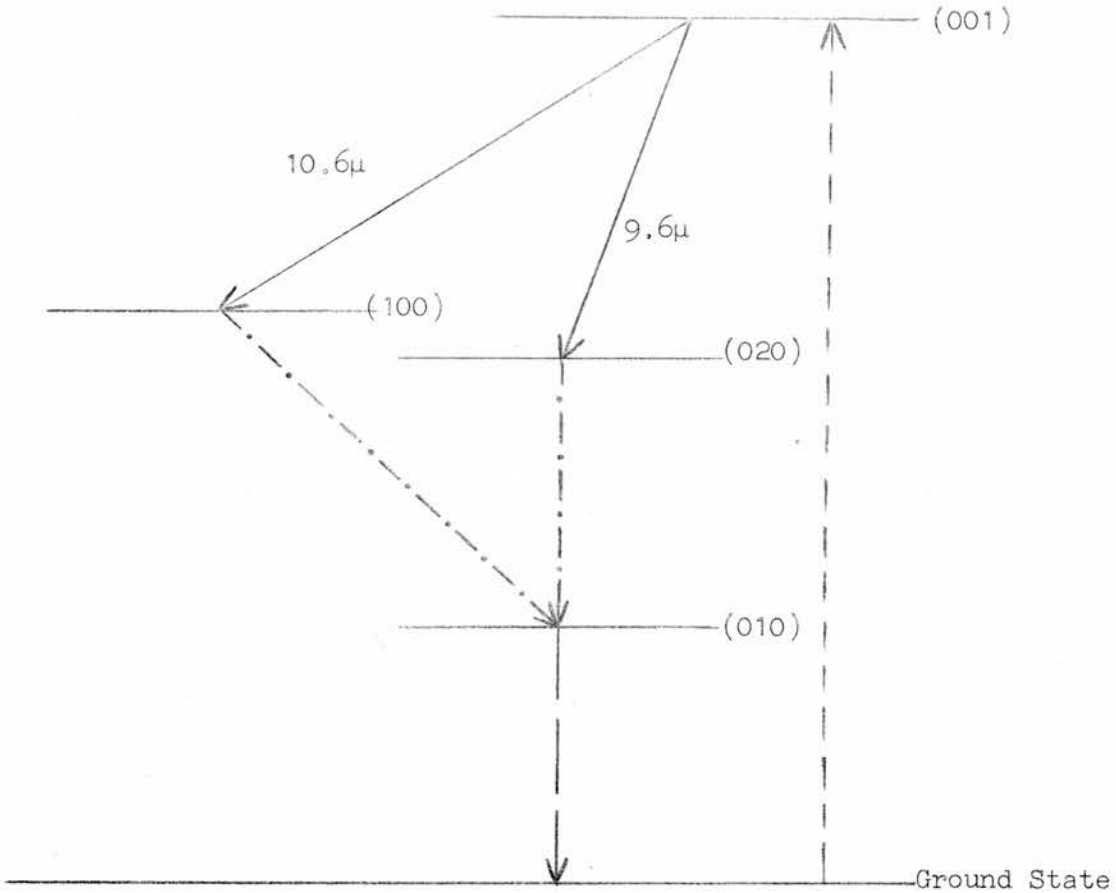

Electron Collision

Resonant Collision with $CO_2(000)$

Stimulated Emission

Inelastic Collision

FIG. 3.3 : Energy levels for the CO_2 molecule

spaced. This reaction can be represented

$$CO_2(00n) + CO_2(000) \rightarrow CO_2(00n-1) + CO_2(001)$$

This process is resonant in the sense that there is redistribution of the energy of the excited molecule without any loss of total internal energy by its conversion into kinetic or thermal energy. The molecules in the $CO_2(001)$ state return to the (100) and (020) states by stimulated emission, and are deexcited into the (010) state by collision with an (000) state. This process is again resonant since the (020) and (100) states have energies about twice that of the (010) state. These transitions are represented

$$CO_2(020) + CO_2(000) \rightarrow 2CO_2(010)$$

$$CO_2(100) + CO_2(000) \rightarrow 2CO_2(010)$$

The (010) state then decays by nonresonant collisions which convert the vibrational energy into kinetic energy. These collisions take place with CO_2 molecules, impurity molecules or the tube walls.

The addition of nitrogen to CO_2 causes a highly selective pumping to the (001) level of the CO_2 molecule, because the first vibrational excited state of N_2 has almost the same energy as the (001) level of CO_2. Also the $N_2(1)$ level is very long lived and approximately 30% of the molecules can be excited into this first

vibrational state. A resonant transfer of energy to the (001) CO_2 state is highly efficient and produces selective pumping of the upper laser state by the collisional reaction

$$N_2(1) + CO_2(000) \rightarrow N_2(0) + CO_2(001)$$

Higher vibrational states of N_2 are also close to the corresponding CO_2 states and resonant transfer occurs into the CO_2(00n) states, which transfer as shown before into the CO_2(001) state.

Additives such as water vapour, helium, hydrogen and carbon monoxide increase the collisional deexcitation of the lower laser states (020) and (100), thus giving rise to increased output. Carbon monoxide also seems to aid the excitation process by changing the electron energy distribution to make it more favourable for exciting the CO_2(001) state. At the present date power output from a continuous CO_2 - N_2 laser is about 80 watts per metre of tube length at a pressure of 3 torr CO_2, 3 torr N_2 and 20 torr of He.

CHAPTER IV - MECHANISMS IN AN ARGON ION LASER

4.1 Introduction.

The energy levels of an argon ion laser can be represented as shown in figs. 4.1 and 4.2. The important transitions can be classed into the types

a) 4p → 4s: these transitions occur with emission of a photon of about 5000 Å. They are primarily of 2 types, one being a transition to a short-lived 4s state with a lifetime of typically 1 nsec, and the other to a long lived metastable 4s state with a typical lifetime of 100 nsec. The transitions which oscillate are mainly of the first type.

b) 4p → 3d: these transitions have a wavelength of about 4500 Å and provide alternative decay paths for ions in the 4p states. The transition at 5017.16 Å can oscillate under certain conditions.

c) 5s → 4p: these transitions pump the upper laser levels by cascade and have a wavelength of about 4000 Å. Transitions from higher s states can be neglected since their contribution is at least an order of magnitude less than that of the 5s states.

d) 4d → 4p: these transitions also pump the upper laser levels and have a wavelength of about 3500 Å. Higher d transitions are again negligible.

e) 4s → 3p, 3d → 3p: these provide the decay path into the ion ground state at a wavelength of about 700 Å in the vacuum ultraviolet. It is possible for this type of radiation to become

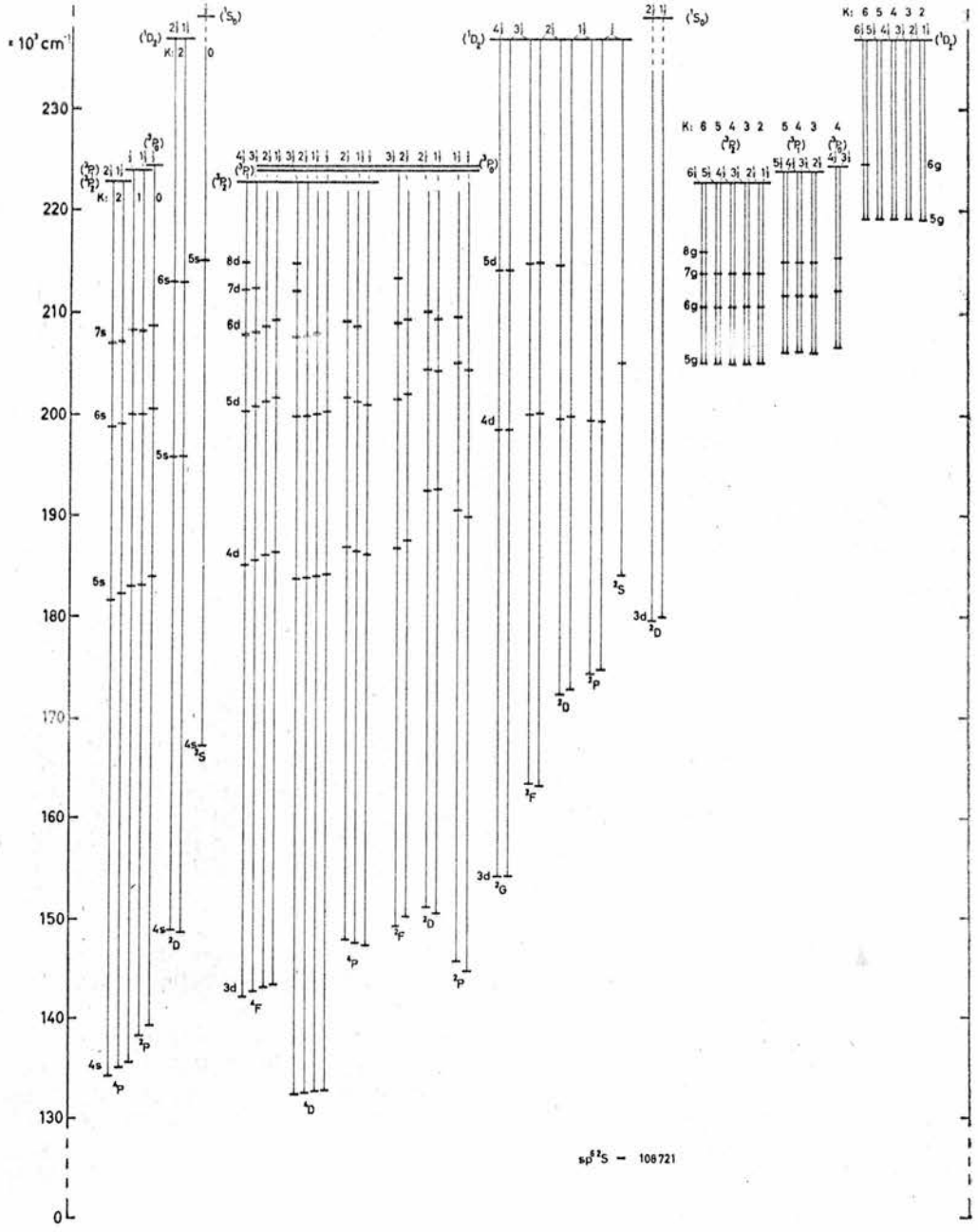

Fig. 4.1: Energy level diagram for the even Ar II levels.

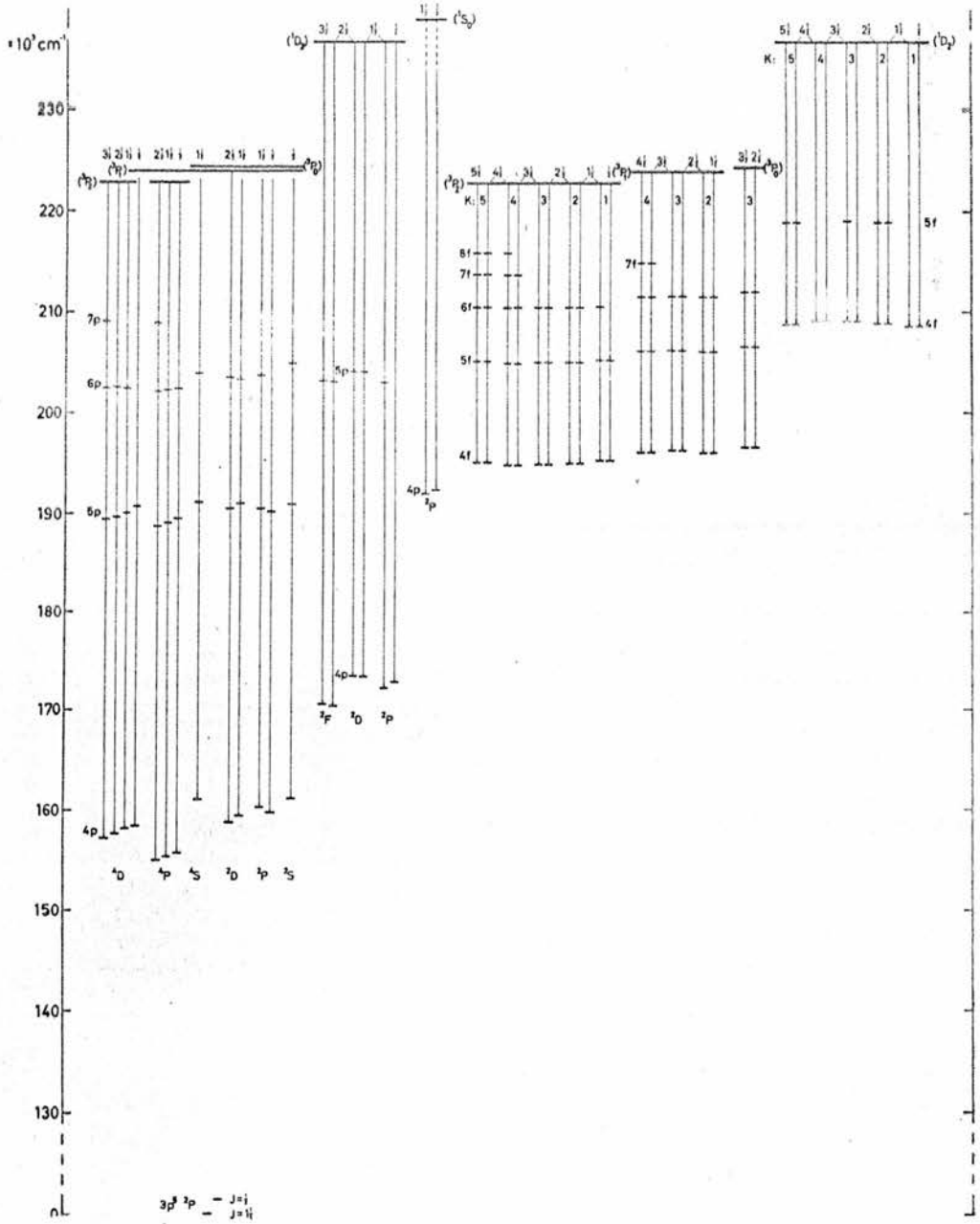

Fig. 4.2: Energy level diagram for the odd Ar II levels.

Wavelength	4764.86	4879.86	4965.07	5145.32	Minnhagen (19)
Upper level	$(^3P)4p\,^2P^\circ_{3/2}$	$(^3P)4p\,^2D^\circ_{5/2}$	$(^3P)4p\,^2D^\circ_{3/2}$	$(^3P)4p\,^4D^\circ_{5/2}$	
Lower level	$(^3P)4s\,^2P_{1/2}$	$(^3P)4s\,^2P_{3/2}$	$(^3P)4s\,^2P_{1/2}$	$(^3P)4s\,^2P_{3/2}$	
Lifetime ($\times 10^9$ sec)	9.4 9.9	9.1 9.7	9.8 9.8	7.5 7.7	Bennett (20) Rudko & Tang (21)
Transition Probability $\times 10^{-7}$ sec	7.15 5.40 4.47	8.96 6.59 8.45	2.63 -- 4.61	0.71 -- 0.92	Statz et al (22) Olsen (23) Rudko & Tang (21)
Pulsed gain (db/m)	> 3.7	3.0	2.8	2.1	Bennett (20)
DC Cascade pump rate (cm^{-3} sec^{-1})	1.78×10^{16}	1.06×10^{17}	7.11×10^{16}	1.37×10^{17}	Rudko & Tang (21)
Branching Fraction	0.67 0.42	0.81 0.49	0.26 0.27	0.053 0.057	Statz & Bennett (24) Rudko & Tang (21)

Fig. 4.3: Available data on argon transitions.

self trapped when the ion ground state population is sufficiently large (see section 4.5).

A synopsis of the available information on the main oscillating transitions, which are the basis of the present investigation, is shown in fig. 4.2. These main lines are the $5145\mathring{A}[(^3P)4p\,^4D^\circ_{5/2}\rightarrow(^3P)4s\,^2P_{3/2}]$, $4965\mathring{A}[(^3P)4p\,^2D^\circ_{3/2}\rightarrow(^3P)4s\,^2P_{1/2}]$, $4880\mathring{A}[(^3P)4p\,^2D^\circ_{5/2}\rightarrow(^3P)4s\,^2P_{3/2}]$ and $4765\mathring{A}[(^3P)4p\,^2P^\circ_{3/2}\rightarrow(^3P)4s\,^2P_{1/2}]$. The mechanisms for the excitation of the 4p ion states to provide a population inversion on the 4p → 4s oscillating transitions can be classified under several headings and these are presented in the following sections.

4.2 Single Step Excitation.

Mechanisms in this group consist of excitation of atoms in the neutral state into the 4p or higher energy states of the ion by one fast electron collision. The higher energy states contribute to the population in the 4p state by subsequent radiative decay.

The single step excitation mechanism is amenable to a theoretical approach known as 'sudden perturbation theory' in which two processes are possible. In the first an incident electron collides with one of the bound electrons, and either of these two electrons collides with a third which is either excited or completely ejected from the atom. Higher order processes (i.e. multiple scattering)

also contribute to this process, but for fast electrons the probability of these is small compared with the primary process. For high enough energies of the incident electron the second process, where the collision takes place in a time very much shorter than the relaxation time of the atom, will occur. Here there is a very small probability of another collision, and the other electrons in the atom are only very slightly influenced by the collision. In the subsequent relaxation process of the ion, there is a finite probability of one of the remaining bound electrons being excited or even ionised.

In 1962 Bennett et al (24) working on the excitation of noble gases when bombarded by α-particles from polonium, was able to interpret the resultant spectra emitted by the gases in terms of a direct excitation process as described above. In 1964 working on super radiance and quasi - cw oscillation in an argon ion pulsed laser (25), he used a 'sudden perturbation' approach to estimate the cross sections for a single step ionisation and excitation of the argon atom. Assuming that the wave functions of the electrons in the ion core are not affected by the 'sudden' collision (i.e. assuming a collision of the type described above), then it is possible to expand the wave function before collision in terms of those of the excited states after collision, and find expressions for the probability of exciting a particular ion state.

This implies that the excited states must have the same parity as the atom ground state and so selective pumping of the levels is possible. The difficulty in this approach is to find proper wave functions for the excited states of argon. Bennett assumed hydrogenic wave functions and an LS coupling scheme for his calculations. These indicated that the $4p\,^2P^o$ states would be strongly populated by this process, and he found that transitions from these states to the short-lived 4s states did indeed provide oscillation. He concluded that the upper states of the other transitions on which he observed oscillation could be populated by a failure of the LS coupling which he assumed.

In 1964 McFarlane (26), studying laser oscillation and UV transitions of singly and multiply ionised oxygen, carbon and nitrogen in high current, pulsed discharges, observed that the general assignments, whether in singly, doubly or triply ionised atoms, involved an upper p state and a lower s state. He had already reported this effect in neon in a previous paper (27), and suggested that preferential excitation under a definite selection rule of the p states, was operative. He applied Bennett's approach to the atoms involved and found the results consistent with his observed upper laser levels in O II and N II. When applied to the production of excited C III and N IV ions by collisions with C II and N III ions in the ground state, agreement was again reached. He failed however to predict levels excited in O III and N III if fast

electron collisions with O II and N II ground state ions were responsible, and interpreted this as a failure of the LS coupling assumed in the calculation.

In 1966 Koozekanani (28) calculated the cross sections for single step excitation of Ne, Ar and Kr by electron collision. He used the same approach as in Bennett's paper (25), but adopted a mixed coupling scheme and wave functions obtained from a computer programme, giving the self-consistent Hartree-Fock wave functions in the Slater approximation. Cross sections for excitation into the 4p states can then be calculated [see fig. 4.4]. It can be seen that the $(^1D)^2P^\circ_{3/2}$ and $(^1D)^2P^\circ_{1/2}$ have the largest cross section but these transitions do not in fact provide oscillation. However oscillation on the next four largest cross sections of the $^2S^\circ_{1/2}$, $^2P^\circ_{1/2}$, $^2P^\circ_{3/2}$ and $^2D^\circ_{3/2}$ states has been observed at 4579, 4658, 4765 and 4965 Å respectively. The 4880 Å transition, which is one of the strongest oscillation lines in argon, is preferentially populated from the 5p $^2P^\circ_{3/2}$ state by cascade via the 5s $^2P_{3/2}$, and about 40% of the ions in the 5p $^2P^\circ_{3/2}$ state decay into the 4p $^2D^\circ_{5/2}$ state, which is the upper level of the 4880 Å oscillation. Since the 5p $^2P^\circ_{3/2}$ is strongly populated then so is the 4p $^2D^\circ_{5/2}$, although not directly.

In 1966 Rudko and Tang (21) concluded that in a system using current densities of the order of 100 A cm^{-2} DC and a pressure of 500 mtorr, the population of the upper laser states was achieved

Upper State		Cross Section relative to ionisation X section X 10^3
^3P	$^2S^o_{1/2}$	0.697
^3P	$^2P^o_{1/2}$	2.723
^3P	$^2P^o_{3/2}$	2.624
^3P	$^2D^o_{3/2}$	1.285
^1D	$^2P^o_{3/2}$	9.338
^1D	$^2P^o_{1/2}$	9.886
^3P	$^4P^o_{3/2}$	0.014
^3P	$^4D^o_{3/2}$	0.014
^3P	$^4S^o_{3/2}$	0.040
^3P	$^4P^o_{1/2}$	0.007
^3P	$^4D^o_{1/2}$	0.014
^1D	$^2D^o_{3/2}$	0.013

Fig. 4.4: calculated cross sections for excitation by a single electron collision in the sudden perturbation approximation.

by multistep or cascade processes and not by single step processes. This gave evidence that the single step process was not significant at low electron energies and this would be expected from sudden perturbation theory. In 1966, Bennett et al (31) produced measurements of single step excitation cross sections in argon using electron beam bombardment of the atoms. Apart from some work on helium (29)(30), these measurements provided the first experimental evidence for absolute cross section measurements of the 'sudden perturbation' process. These cross sections became appreciable for incident electron energies of > 40 eV. The effects of cascade on the measurements was taken into account, by observing that the $4p\ ^4D^o_{5/2}$ upper state of the 5145 Å transition would be populated largely by cascade, since no excitation of this state is allowed on the sudden perturbation approach. A rough measure of the cascade contribution is therefore obtained and correction of the determined cross sections gave results which agreed with the previous theoretical values of Koozekanani (28).

In 1967, Vainshtein and Vinogradov (32) used the sudden perturbation approach with LS coupling and a semiclassical theory, to calculate the cross sections for direct excitation of the excited states of the argon ion. They obtained qualitatively similar results to their previous method using the first Born approximation (33), but found that their values were smaller than

Bennett's measured values (31). This is explained on the basis of the cascade contribution as previously mentioned. They found the cross sections to increase rapidly for electron energies of > 40 eV.

The most recent paper from Koozekanani (34) contains a comparison of the relative importance of a direct single step excitation of the argon ion 4p states from the neutral argon metastable 4s states, to a two step process from the same 4s states via the ion ground state. The basis of choosing the metastable 4s states as the initial states, is that they have an ionisation threshold of only 4 eV, and a cross section of nearly ten times that of the ground atomic state. He uses a 'sudden perturbation' approach to estimate the cross section of the one step process, and takes into account the fact that only states with a ^3P core configuration are important for laser action. The resultant cross section is $Q_E = 8.1.10^{-3}\ Q_i$ where Q_i is the ionisation cross section from the 4s metastable states. He eventually obtains the ratio of the number of ions excited directly (N_d) to the number excited via the ion ground state (N_i) to be

$$\frac{N_d}{N_i} = 8.10^{-3} \frac{\langle Q_i v \rangle N_m}{\langle \sigma v \rangle N_i} \qquad (4.2.1)$$

where N_m = density of metastable states

N_i = density of ions

v = velocity of electrons

σ = excitation cross section from ion ground state to 4p state

<> denotes taking the average over the electron velocity distribution

Now $Q_i \sim 10\sigma$ and the threshold for ionisation from the metastable state is $\sim$ 4 eV, whereas the threshold for excitation from the ion ground state is $\sim$ 15 eV, therefore $\langle Q_i v \rangle >> \langle \sigma v \rangle$, and this could compensate for the factor 10^{-3} assuming the metastable density is high enough. The direct excitation process would then become more important.

The evidence to date is that the direct excitation mechanism is important at high electron energies such as would be found in high current pulsed discharges, but that in lower current CW devices other processes, such as multistep excitation, are the dominating mechanisms. It will be shown in Chapter VII that single step excitation provides an explanation of the observed behaviour of the spontaneous emission at high current densities.

4.3 Multistep Excitation.

Multistep excitation in the argon ion laser can be of several types, since the neutral atom can be excited stepwise through the metastable 4s neutral atom levels fig. 4.5(a), the ion ground state fig. 4.5(b), the ion 3d or metastable 4s states fig. 4.5(c) or the 4d and 5s ion excited states fig. 4.5(d). Some of these processes

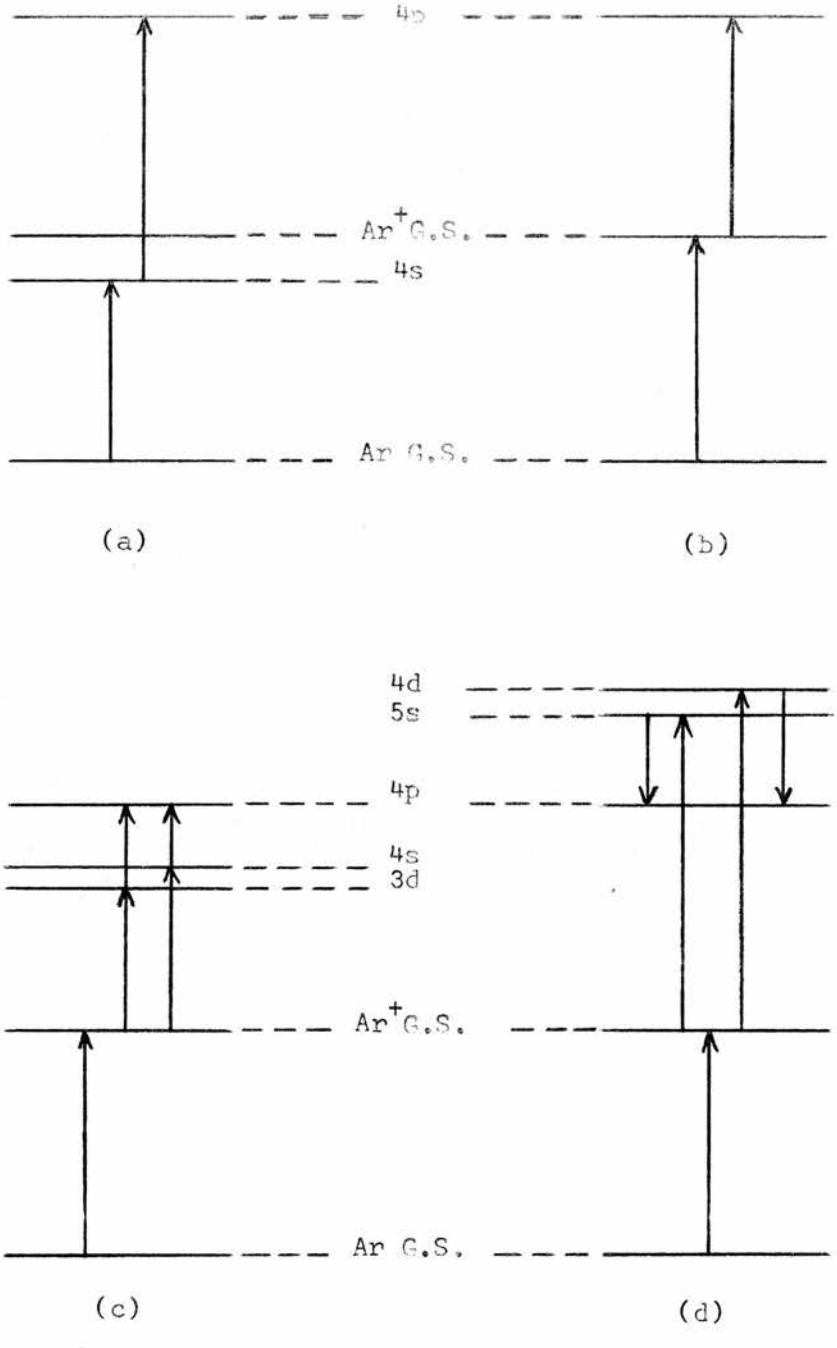

Fig. 4.5: Multistep excitation mechanisms.

can also be taken with subsequent cascade to give a contribution to the population of the 4p states.

Gordon et al (35) proposed an excitation from the argon ground state into the 3p argon ion ground states by an electron collision, and then by a further electron collision into the 4p states. They base this mechanism on the fact that the intensity of the spontaneous transitions in the ion states, are dependent on the square of the discharge current. It is also worth noting that a mechanism of this type, which does not involve an intermediate metastable level, would not provide a 'bottleneck' or saturation at high currents. However any two step process would give quadratic dependence on the current, provided the dominant relaxation rate of the intermediate state is independent of the discharge current.

Bennett and Lichten (36) proposed excitation of the ground state atom by electron collision into the 4s metastable levels of the neutral atom, and subsequent excitation, again by electron collision, into the 4p or higher states of the ion. This process again provides quadratic dependence of the spontaneous emission on discharge current. The first step of this reaction has the highest neutral excited state cross section, whereas the second step would favour the production of 4p states due to the selection rules. This process can be treated as a 'sudden' process and has therefore been included in section 4.2 on direct excitation

mechanisms using a sudden perturbation technique for analysis.

Miller et al (37) conclude from their experiments on a 2mm bore tube operating CW at a current density of about 100 Acm^{-2}, that the mechanism of direct excitation from the ion ground state or the 4s metastable ion states is the most important one. This mechanism would lead to a quadratic dependence of the spontaneous emission on current density, and so is compatible with the widely observed spontaneous light behaviour at low current densities. The present set of measurements also show that under pulsed conditions the quadratic dependence is followed for low current densities. Further information on the importance of the electron collision contribution from the 4s metastable ion states is available in the work of Beigman et al (38) in which the collision cross section for the 4s → 4p transition is given as about 8.10^{-12} cm^2 at an electron temperature of 10^5°K. A large population is expected in the 4s metastable states because of their relatively long lifetimes. Cross-sections for collisional excitation from the 3d ionic states are a factor of 4 less than those for the 4s metastable states (38) and the radiative lifetimes of the 3d states are shorter than those of the metastable 4s states, so this contribution will be about an order of magnitude less than the electron collisional excitation from the 4s metastable states.

The mechanisms of the foregoing type, which excite ions into the 5s, 4d and higher states and indirectly then populate the 4p levels by cascade, have been treated collectively in section 4.4 on cascade processes.

4.4 Cascade Processes.

Cascade contributions to the pumping of the upper laser states come from the energy states lying higher in the energy configuration of the excited ion. The upper laser levels have a 4p upper state, so that any states of higher energy (e.g. 5s, 4d etc.) can contribute to their population by decaying into the 4p state, and emitting a corresponding energy photon. The importance of this contribution depends on the conditions occurring in the laser, but it must always occur to a certain extent and the photons emitted in the cascade appear as spontaneous emission. As most of the transitions 4d → 4p, 5s → 4p, 4p → 4s and 4p → 3d are in the range 3000 Å - 5000 Å the argon discharge has a characteristic blue colour.

In 1966 Statz et al (22) looked at the relative importance of cascade from the upper states of the argon ion into the 4p upper laser state. Using the spontaneous emission measurements by Minnhagen (19), they added the cascade contributions from each state into a 4p state and plotted the results as in fig. 4.6. This shows that the 4d states contribute most to the 4p state

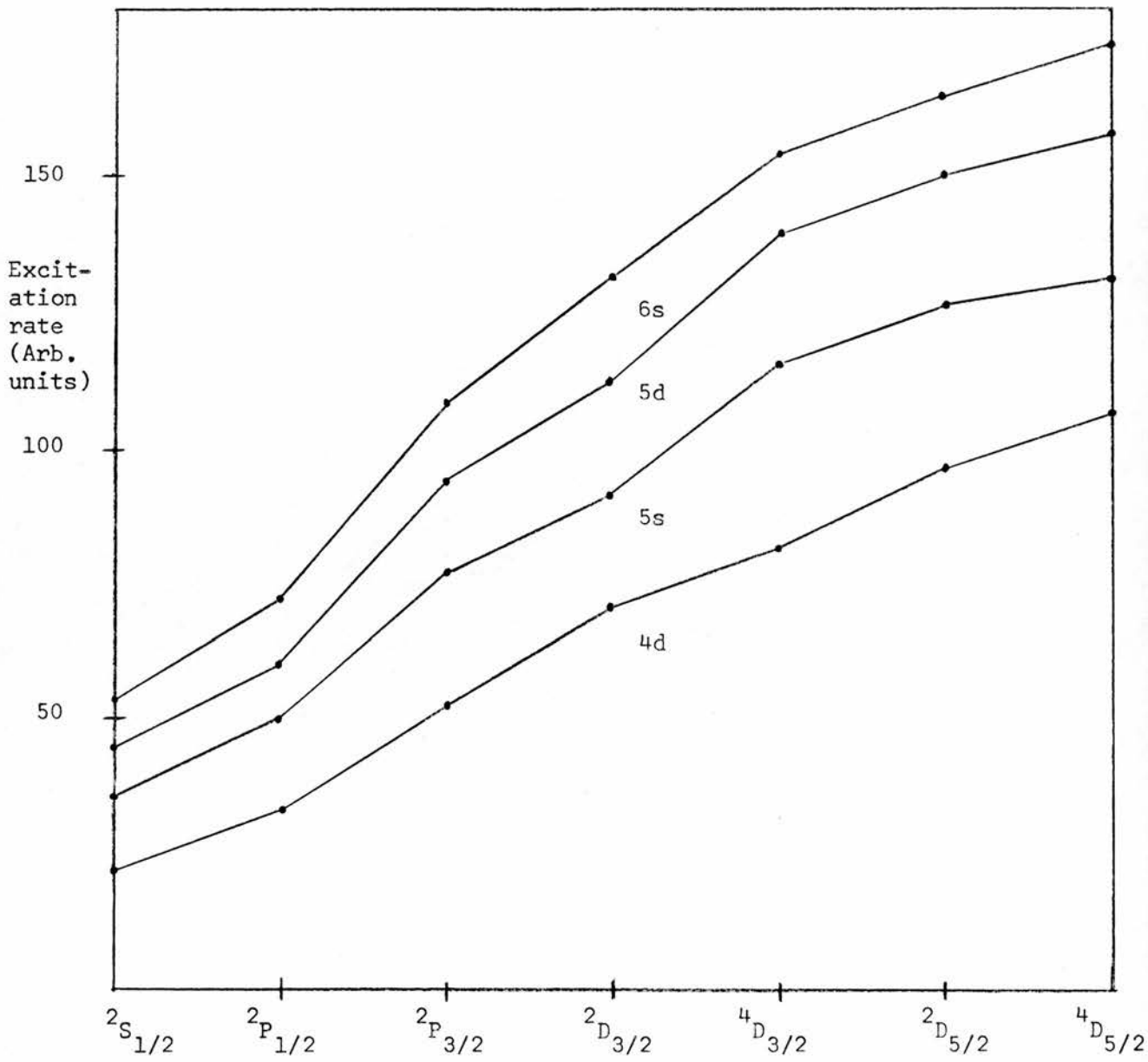

Fig. 4.6: Cascade contribution to population of 4p states.

population and that the levels in the 4p states, receiving most cascade pumping, are the $^2D^\circ_{5/2}$ and the $^4D^\circ_{5/2}$. These two levels form the upper laser states of the two most prominent oscillation lines in argon viz. the 4880 Å and the 5145 Å. Noting that the 4d levels provided the major contribution, they calculated theoretically their contributions to the 4p state population assuming that all the 4d levels were excited at the same rate. The results agreed reasonably with the experimental determination and again showed preferential pumping of the $^4D^\circ_{5/2}$ and $^2D^\circ_{5/2}$ levels.

In 1966 Rudko and Tang (21) obtained evidence lending support to the theory that the upper laser levels derive a large part of their population indirectly by cascade from upper levels. Using a 1 mm diameter tube and current densities $\sim$ 100 Acm^{-2} they measured the total intensities of all the stronger spontaneous emission lines terminating on the 4p $^2D^\circ_{5/2}$ state of the argon ion. This is, of course, the upper state for the 4880 Å laser transition. Their results compared favourably with those of Minnhagen (19), who had used different discharge conditions. They then calculated the total power radiated by the entire gas in one spontaneous line (4013.86 Å), assuming isotropic radiation, and computed the total rate of supply of ions (g) into the 4p $^2D^\circ_{5/2}$ state. It was found that g varied quadratically with current up

to current densities of about 200 Acm^{-2}. Using a simple assumption of a Doppler broadened line, they deduced the dependence of the output laser light in the 4880 Å transition on current and found good agreement with experiment.

Bennett et al in 1966 (31) measured the cross sections for direct electron excitation of the 4p states and found values larger than theoretical values by Koozekanani (28). This is the direction of error to be expected by cascade contribution and they estimated this error assuming the upper state of the 5145 Å line could only be populated by cascade, on the basis of the selection rules. Their measured values agreed fairly well with theory on application of this correction and showed the cascade contribution to be significant at current densities of $\sim$ 100 Acm^{-2}.

In 1966 Koozekanani (28) calculated cross section values for direct electron collision excitation and ionisation of the neutral argon atom, and found that the 4p $^2D^o_{5/2}$ state would not be pumped directly. Another state the 5p $^2P^o_{3/2}$ would however be strongly pumped by this mechanism and he postulated a large cascade contribution from the 5p $^2P^o_{3/2}$ to the 4p $^2D^o_{5/2}$ state via the 5s $^2P_{3/2}$ state. This is illustrated in fig. 4.7, showing the relative transition probabilities as percentages of the total transition probability. Note that the 5s $^2P_{3/2}$ level has a lifetime of only 5 nsec.

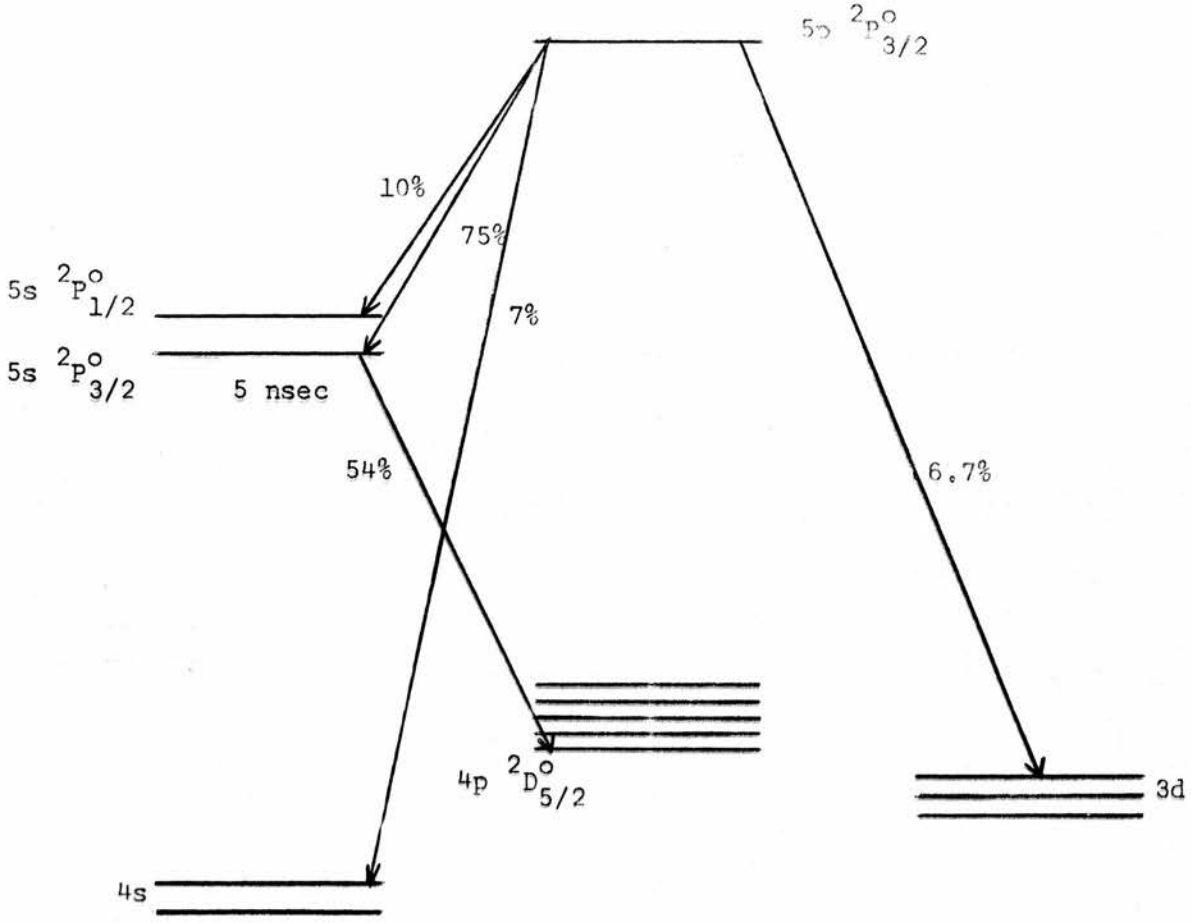

Fig. 4.7: Population of 4p $^2D^o_{5/2}$ state from 5p $^2P^o_{3/2}$ by cascade.

In 1967 Rudko and Tang (21) published the spontaneous intensities for all the important cascade transitions into the 4p states from the 5s and 4d states, in a 2 mm diameter tube with a current density of about 100 Acm^{-2}. They calculated the population densities of the upper laser states, and suggested that in typical DC argon discharge conditions cascade contributions to the upper laser state populations were the dominating mechanism.

The latest paper by Vainshtein and Sobolev (38) gave a calculation of the relative contributions from various excitation mechanisms and found the cascade contribution from the 4d → 4p states to be ∿ 30% of the indirect pumping from the ground state of the argon ion at electron densities of ∿ 10^{14} cm^{-3} and temperatures ∿ 5.10^{4}°K.

The consensus of published work indicates that cascade contributions to the 4p upper laser levels come mainly from the 4d and 5s states and are very important contributions to the population of the 4p states. This process strongly pumps the upper levels of the 4880 Å and 5145 Å lines which are the two strongest laser lines containing about 80% of the total laser output power in a typical discharge. This contribution has been found to be important at lower current densities and it will be shown that the results of the present investigation show that cascade and multistep excitation are the main mechanisms at current densities below about 1500 Acm^{-2}. (See Chapter 7).

4.5 Resonance Radiation and Radiation Trapping.

The term 'resonance' is applied to radiation emitted by an atom or ion in an optical transition from an excited state to the ground state. One of the most common examples of this is the sodium D doublet (5890 and 5896 Å). This resonance radiation is highly absorbable by the gas in its normal state due to the large population in the ground state. Compton (39) treated the transfer of resonance radiation as a type of Brownian motion and obtained a diffusion type equation for the density of excited atoms, thus enabling him to define a diffusion coefficient in terms of the mean free path of the quantum. This treatment neglects to take account of the fact that the absorption coefficient in fact varies over the frequency distribution of the resonance quantum. This broadening can be of three types [1) natural 2) Doppler and 3) Lorentz] (see section 2.3) and each case must be treated differently. Holstein (40) considered an infinite slab of material taking broadening into account and obtained reasonable agreement with values for the rate of decay of excitation measured by Zemansky (41) in mercury vapour. The advantage of Holstein's theory was that no assumption of a mean free path is required and, in fact, he showed that no mean free path could be assumed, because of the strong variation of the absorption coefficient near a resonance line. The decay of the resonance radiation (N) was

described by

$$N \propto e^{-gAt}$$

where

$$g = \frac{1.6}{K_o a \sqrt{\pi \log_e K_o a}} \quad \text{and} \quad K_o = \frac{\lambda^3 N_o}{8\pi} \cdot \frac{g_e}{g_o} A \sqrt{\frac{M}{2\pi KT}} \qquad (4.5.1)$$

The quantities required are A - transition probability between ground state and 1st excited state.

λ - wavelength of this transition.

N_o - population density of ground state.

g_e, g_o - statistical weights of ground and excited states.

M - mass of atom.

KT - Boltzmann energy.

The radiation trapping effectively increases the lifetime (τ) of the 4s lower laser states to $\frac{\tau}{g}$. The effect will thus be appreciable for values of $g < 1$. Substitution in equations (4.5.1) of typical values for a pulsed laser discharge gives $N_o \sim 2.10^{15}$ ions cm^{-3}, for the trapping effect to be appreciable. This density is quite possible for a pulsed laser of the type described later where the current density ~ 3000 Acm^{-2}.

It can be seen that resonance trapping would form a mechanism which would effectively increase the lifetime of the 4s ion states and thus cause their population to increase to destroy the inversion between the 4p and 4s laser transitions. It should be noted that g is an inverse function of the atom temperature T (see equation 4.5.1) and consequently as the gas temperature increased the radiation trapping would become less effective. This is sometimes known as Doppler removal of the resonance trapping process. The increase in the effective lifetime of the 4s states would cause some other decay mechanism to become dominant (e.g. diffusion). Diffusion to the walls and subsequent recombination as the dominant decay mechanism would yield a maximum inversion density varying inversely as the third power of the diameter of the tube, whereas a volume loss mechanism involving collisional destruction of the 4s states would vary inversely with the diameter (42). It is worth noting that the 4s ion levels have lifetimes of $\sim$ 1 ns (i.e. the 4s lower laser levels) and even if radiation trapping increases this by an order of magnitude to $\sim$ 10 ns, the ion velocities of $\sim 10^{5}$ cm sec^{-1} would only be sufficient to move the ion a distance of $\sim 10^{-3}$ cm before radiative decay is probable. This distance is about 100 times smaller than the typical tube diameters involved (1 - 10 mm), so it is unlikely that diffusion limiting is going to be significant. It is interesting to note that an inverse diameter

dependence of the inversion population has been found to occur on a number of four level systems (43). This would indicate volume collisions to be a significant mechanism if the radiative decay is impeded by trapping.

Evidence for radiation trapping in ion lasers was obtained by Bloom et al (44) in 1964 and later by Cheo and Cooper (45) in 1965, when they observed that the output pulse of the laser showed a ring shape instead of a circular shape. This was caused by the quenching of the inversion along the axis of the tube due to radiation trapping, and was shown not to be caused by selective pumping of the upper laser levels by the lower energy electrons near the walls. The onset of this phenomenon occurred at a current density of about 8000 Acm^{-2} and pressures of about 10 mtorr. The effect increased as the current and/or the pressure were increased.

An experiment by Gordon, Labuda et al (37) showed that the 'bottleneck' induced by radiation trapping was removed by an increase in the Doppler width of the ionic transitions. They varied the gas temperature at the beginning of the pulse and showed that absorption on the resonance transition decreased as the temperature increased.

In a paper presented at the 1968 Quantum Electronics Conference in Miami, Klein (46) showed that the radiation trapping theory adequately explains the time behaviour and current saturation of

the pulsed ion laser. His apparatus consisted of an ion chamber built on the end of the laser tube and used the measurement of the positive ion current and the known photo-ionisation cross sections, to find the absolute intensity of the resonance lines.

4.6 Collisional Deexcitation.

The upper laser states can be destroyed by a collision between the excited ion and a neutral atom, or by the collision of an electron with the excited ion. This provides a method of de-exciting the upper laser states without subsequent radiation, and would tend to reduce the power output of the laser. Experiments done by Bennett et al (47) have shown that the former contribution to the decay of the 4p states is negligible in the range 10 mtorr to 2 torr. The decay of the upper Ar^+ laser states after bombardment by threshold energy electrons was shown to depend very little on pressure in the range indicated. By fitting a decay rate of the form of a constant plus a linear pressure term to the experimental results, it was deduced that the cross sections for collisional deexcitation of the 4p ion states by neutral atoms were of the order 5.10^{-15} cm^2. This gives a rate of deactivation of about 10^5 sec^{-1}, which is three orders of magnitude down on the radiative decay of about 10^8 sec^{-1} from the 4p ion states.

Deactivation of the 4p ion states by electron collisions is not however negligible. Beigman, Vainshtein et al (38) calculated

the average cross sections for transitions between the excited states of the argon ion caused by electron collision. They calculated the average value of the product of velocity and cross section to be 8.10^{-7} cm^2 sec^{-1} for the 4s - 4p transition at an electron temperature of 10^5°K. Previous indications (48) show that the electron temperature is probably of this order in the type of laser used in the present work. Assuming an electron concentration of 10^{15} cm^{-3} gives a deactivation rate by collision of 8.10^8 sec^{-1}. This is certainly competitive with the radiative decay rate at high electron densities, and is a process which cannot be neglected. The cross section results used for the calculation have not yet been verified by any other method. The approximation used for their calculation was a Born-Coulomb approximation in which the external electron is described by continuous spectrum Coulomb wave functions. The effective cross sections are then almost independent of the coupling scheme of the atomic electrons, because only groups of levels are considered and not individual levels. The values also assume a Maxwellian velocity distribution for the ions. It must be remembered that the excitations from the 4s states into the 4p states will be significant as well as deactivation collisions, since the 4s metastable population will be an order of magnitude larger than the 4p population. The exact way in which these terms compete will depend largely on the electron energy distribution. If collisional

excitation of the 4p states from the 4s metastable states and collisional deexcitation of the 4p states into the 4s states become the dominant mechanisms, then the ratio of the populations in steady state would be independent of the electron density, and thus independent of the current density. Since the population of the 4s metastable states would be dependent on the electron density, then the spontaneous emission from the 4p states would become linear with current density. This is a possible explanation for the variation of the spontaneous emission dependence on current density which will be shown in the experimental section 7.2.

Collisional deexcitation of excited ions with neutral ions will be of the same order as the contribution due to neutral atom collisions, and so will be neglected in the discussion.

CHAPTER V - EXPERIMENTAL APPARATUS

5.1 Construction of laser tube.

The 3m long laser tube was constructed by joining three fused silica tubes 1m long with a bore of 4mm. These were joined on a glass blower's lathe to maintain good alignment of the tubes. The tube was mounted on clamps, which were held on a 4m long steel girder (see fig. 5.1). When a discharge is passed through this tube there is a tendency for the gas to be pumped by the discharge to one end of the tube, causing a pressure gradient (49), so a return path was provided by adding a 1cm bore cataphoresis tube between the electrodes at either end of the tube. Glass coils were used both in the cataphoresis tube and from the vacuum system to the laser, to prevent the discharge from running through the cataphoresis tube or the pumping tube, in preference to the laser tube. The vacuum system was connected to the cathode end of the discharge tube.

The laser tube was aligned by a taught thread through the tube. The thread was then removed and the windows cemented into place at the Brewster angle with low vapour pressure cement. During operation the discharge dissipates 5-10 KW but natural convection is sufficient to remove this without allowing the temperature of the fused silica to rise above its melting point.

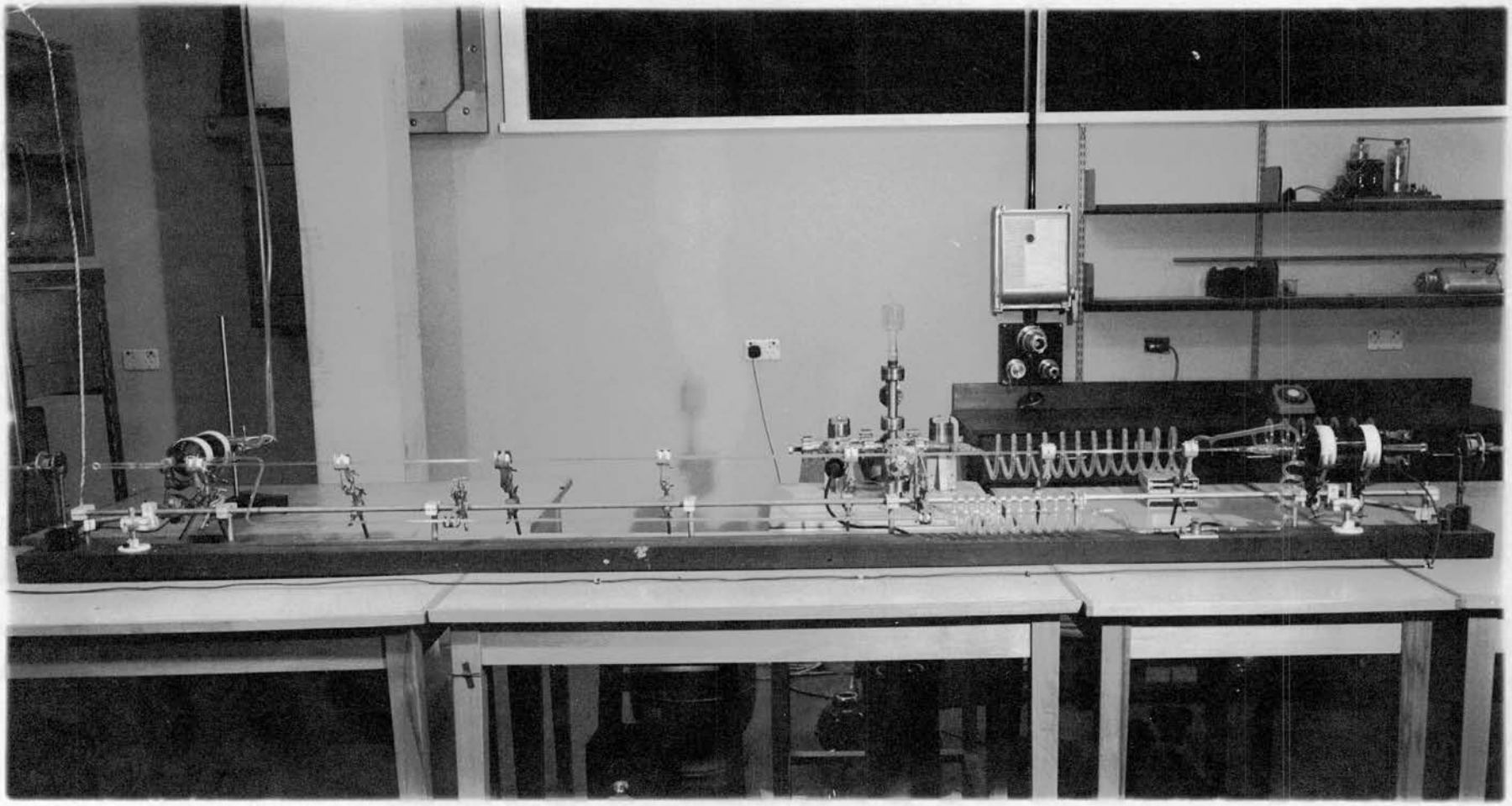

Fig. 5.1: The completed laser.

The anode and cathode construction is shown in fig. 5.2. The anode is a coil of copper tube with a 3mm internal bore. This is brazed into nilo-K to glass seals and joined to the anode envelope with graded seals. The anode is water cooled to prevent overheating of the graded seals during operation. The cathode is a Mullard oxide coated thyratron gun (type XR1-12A) requiring 20 amps at 2.5 volts for the heaters. The heater connections enter the glass envelope by nilo-K to glass graded seals as in the anode construction. Before use, the cathode must be processed under vacuum to activate the oxide coated surface and thereafter kept in an inert gas atmosphere to prevent destruction of the coating material.

The mirrors used to form the cavity were hard coated multi-layer dielectric mirrors with reflectivities of 95% and 99.9%. They were peaked for a wavelength of 4880 $\mathring{A}$ with a bandwidth of 400 $\mathring{A}$. The radius of curvature of both mirrors was 2m, and, since they are positioned 3m apart, they form a low loss type of cavity intermediate between a confocal system and a concentric system (50). The mirrors were held in an adjustable holder and clamped to the girder by magnetic clamps. The mirrors were aligned by three screws on a system which provides movement about any axis.

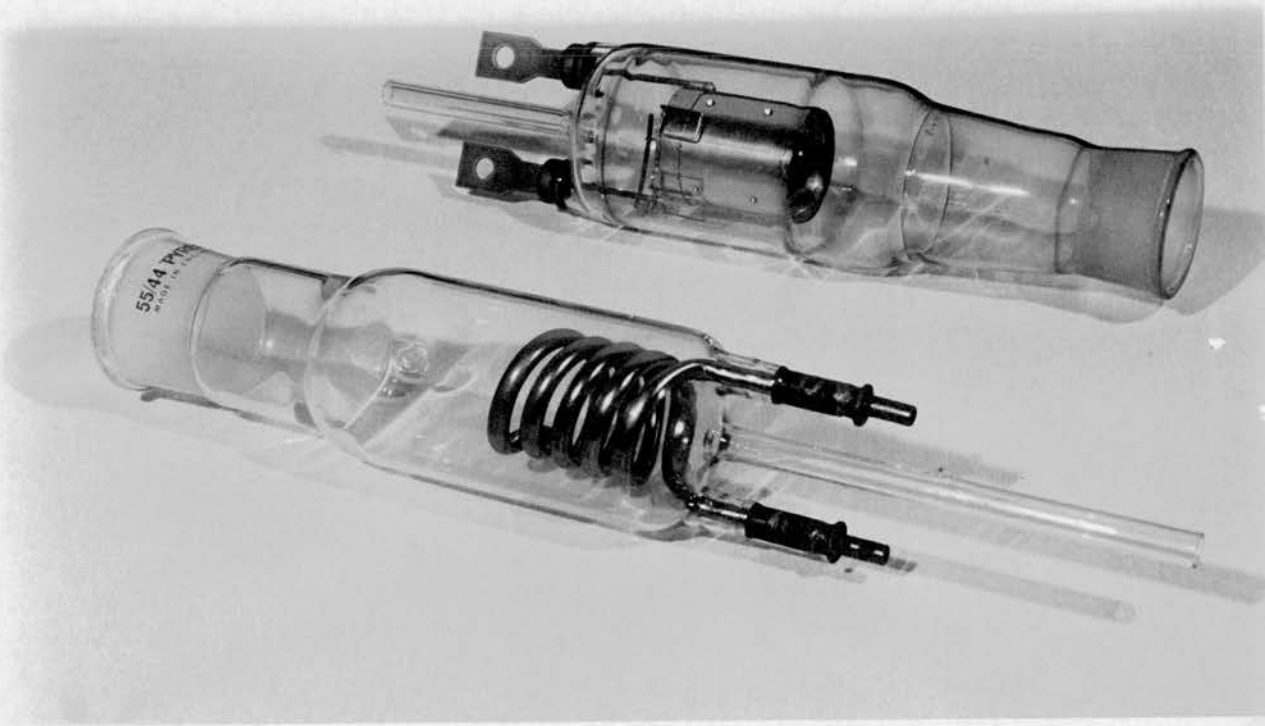

Fig. 5.2: The copper coil anode and oxide coated cathode.

5.2 Vacuum System and Pressure Gauge.

The laser is pumped by an adsorption pump which contains zeolite cooled to liquid nitrogen temperatures. This material adsorbs the molecules of the gases onto its surface and retains them until it is allowed to warm up to room temperature. The pump incorporates a one way safety pressure valve which allows the adsorbed gases to escape into the atmosphere whenever the pressure inside the pump exceeds one atmosphere. The ultimate pressure of this pump, which has a speed of 8 litres/sec, on the system with a volume about 10 litres, is 2 mtorr. When this pressure is reached an ion pump can pump the system to about 10^{-5} mtorr to ensure cleanliness, before the laser is filled with spectroscopically pure Argon gas (BOC grade X) to the required pressure of about 40 mtorr. The system had to be pumped for several days initially to reach the required pressure when the system was first cleaned.

Pressures in the range 5-500 mtorr were measured with an Edwards pirani type vacuum gauge model 8/2, and pressures below 5 mtorr by a Vacuum Generators ion gauge type IGP 1. These gauges can be corrected to read pressures in pure Argon although they are calibrated for dry air. To convert the pressure read on the instrument to the true pressure in argon it is necessary to multiply by 1.6 in the region of 50 mtorr.

5.3 Laser Power Supply.

An eight section transmission line consisting of 0.001μF capacitors and 2mH chokes is formed with a characteristic impedance chosen to match the impedance of the discharge tube approximately. Matching enables power to be transferred into the discharge with minimum reflection back into the circuit. The capacitors are charged by a resonance method (51) through a diode and charging choke, from a 10KV DC power supply (see fig. 5.3). This supply rectifies 3 phase power to provide the DC supply. Triggering of the circuit is provided by a thyratron English Electric FX229, which is triggered from a 1.5KV pulse unit of variable frequency. The supply can transfer pulses of variable voltage at current densities of up to 6000 Acm^{-2} into the 4mm bore laser tube. The breakdown characteristic of the laser tube is shown for both cold cathode and heated cathode operation in fig. 5.4. It will be noted that the tube breaks down at about 750v, so that in normal running the tube has about five times this voltage applied to it and will be easily broken down to start the discharge. Using the current and voltage measuring devices (see section 5.4) it was possible to determine the impedance of the tube at different pressures. This is shown in fig. 5.5 for pressures of 40 mtorr and 50 mtorr. The graphs are practically linear implying that the tube impedance is roughly constant, and the slope corresponds to a tube impedance of about

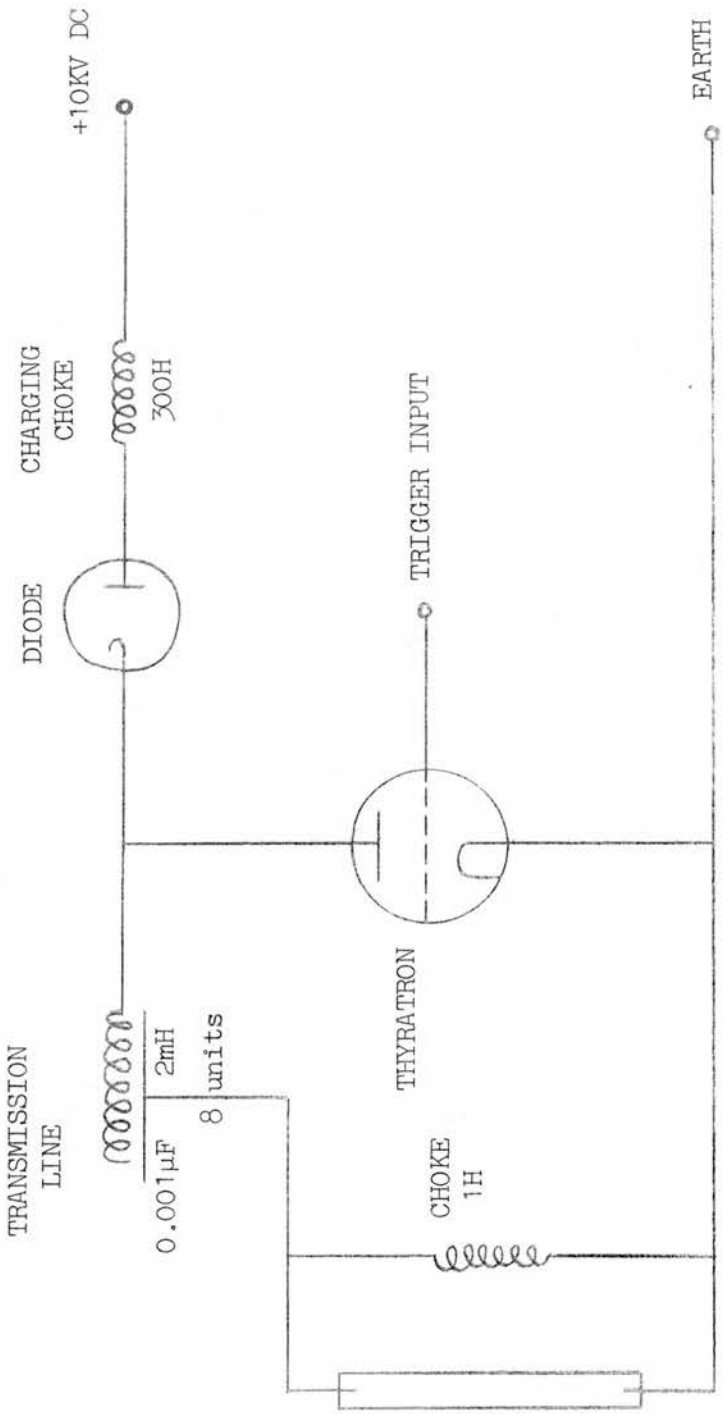

FIG. 5.3 : Resonance charging network for argon ion laser.

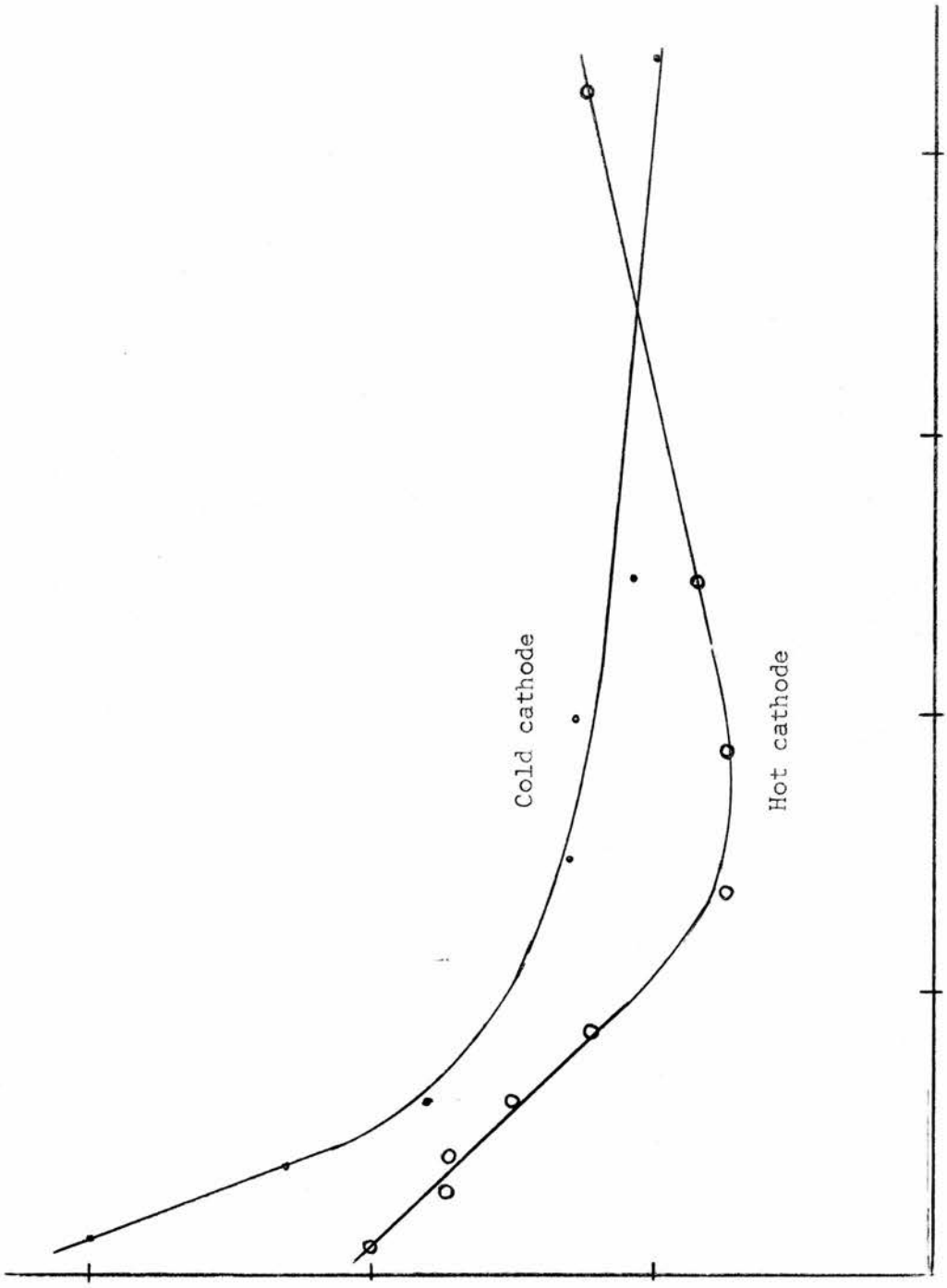

Fig. 5.4: Breakdown voltage of laser tube.

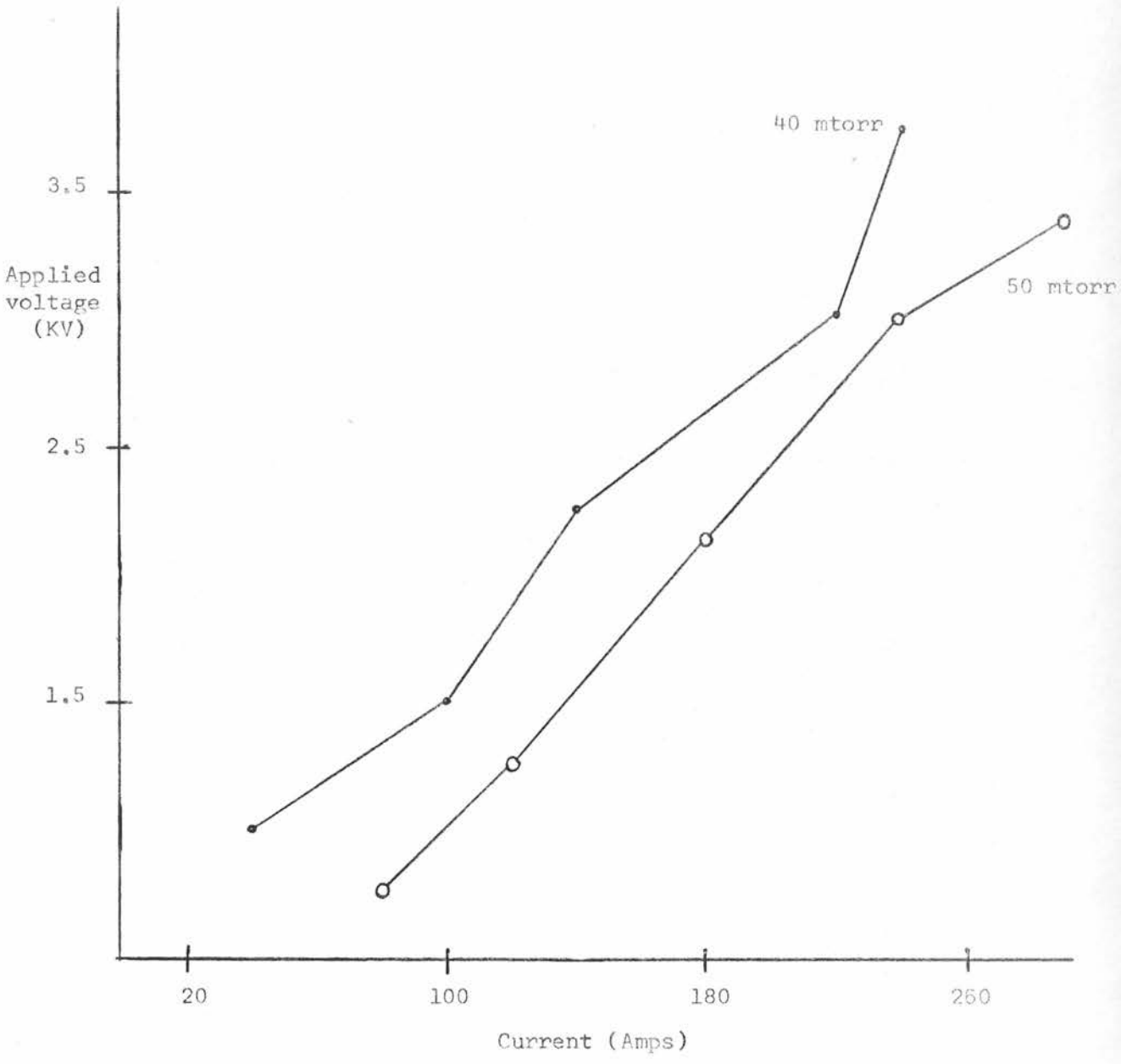

Fig. 5.5: Impedance characteristic for laser tube.

15Ω. This is further borne out by the fact that inclusion of a 15Ω non-inductive resistor in series with the tube halves the current through the tube. The general shape of the current pulse can be seen in the photographs shown as fig. 7.3 in Chapter 7.

5.4 Time-resolved current and voltage measurement.

The current measurements were made with an inductive probe Tektronix type P6016 used with a passive termination. Sensitivity can be selected at 2ma/mv or 10ma/mv with 3% accuracy, and risetime is 18 nanoseconds, when used with a type L plug in. Typical delay time is 12 nanoseconds at the 50% level of pulse amplitude, and insertion impedance for 1 μsec pulses is about 0.014Ω. The passive termination for sensitivity of 2ma/mv is shown in fig. 5.6.

The voltage applied to the tube is measured using a low inductance carbon resistor potential divider. This enables the time resolution of applied voltages of about 10KV peak values by introducing an attenuation factor of 60 so that the pulse can be displayed on the oscilloscope and photographed.

5.5 The Image Converter Camera.

The camera used for recording the time resolved behaviour of the stimulated emission output of the laser is an STL Image

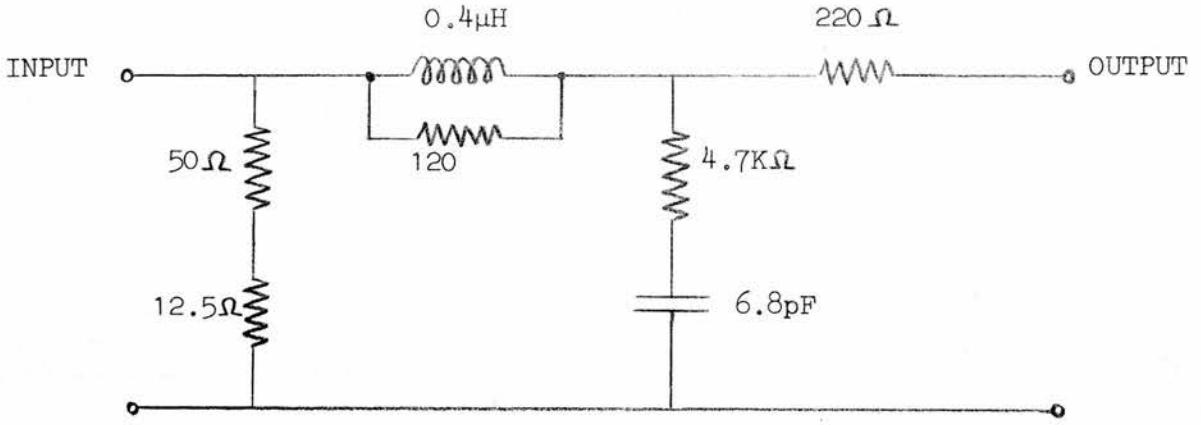

FIG. 5.6 : Current probe termination.

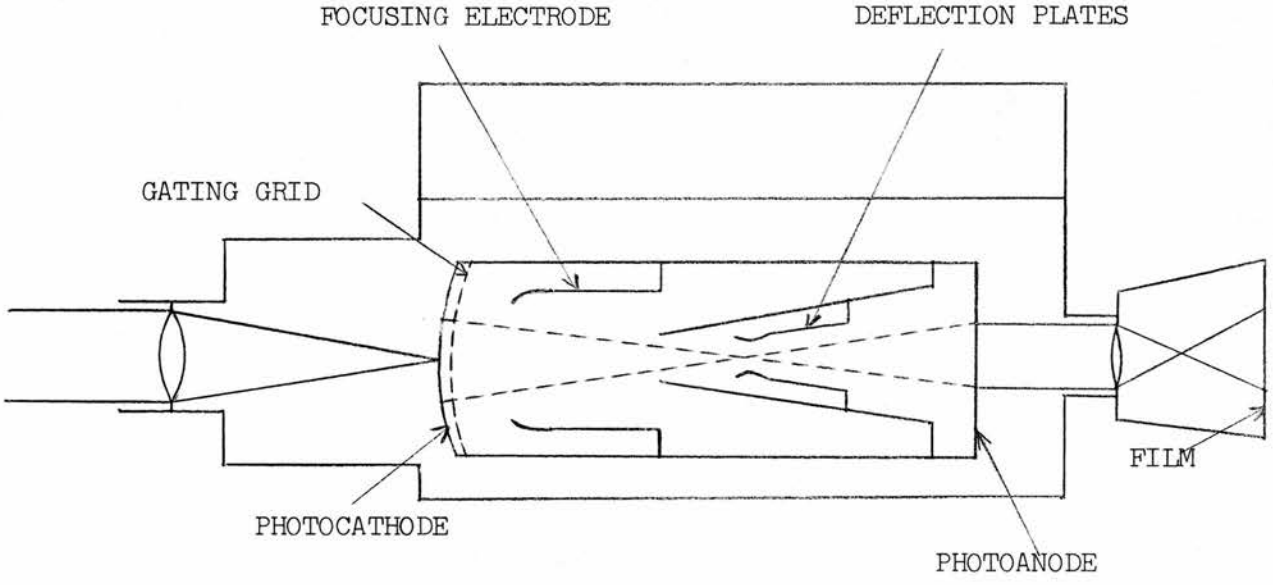

FIG. 5.7 : Schematic diagram of Model 1D Image Convertor Camera.

Converter Camera Model 1D used in the streak mode. Several plug-in facilities are available for this model, but it is used here with the wide range streak unit model 5B giving writing rates of 100, 50, 25, 10 and 5 millimetres per microsecond on the film. The camera produces streak pictures on polaroid type 410 (10,000 ASA) film with a corrected STL Elgeet Navitar f/2 125mm focal length objective, and a corrected STL Elgeet Navitar f/1.2 85mm focal length rear lens system. This system gives a field of view of 9" x 6" at a distance of 3' from the camera. A diagram of the camera head is shown in fig. 5.7. Light entering the objective falls on the photocathode and produces photoelectrons with a density corresponding to the light intensity at that point. This 'electron image' carrying the picture information is gated, focussed and deflected by internal electrodes and accelerated onto the photoanode, which reconverts the signal into light which can be observed and photographed.

The effective shutter of the arrangement is the gating grid which is controlled by its voltage with respect to the photocathode. The beam is cut off when the grid is at -90v and needs a positive voltage of 160v to turn on the beam. The transmission ratio of shutter open relative to shutter closed is better than 10^6. For streak photography a ramp voltage is applied to one deflection plate and the image is streaked linearly downward across the screen, while the gate is open. The sweep is timed to begin

before the gate pulse and last longer, so that none of the picture information is lost.

The streak camera requires a trigger pulse of 300v with a rise time of 10 nanoseconds to start the streak and this is provided by a Model 2A Trigger Delay Generator (TGD). This unit enables the camera to be triggered either optically or electrically and also allows any delay from 10 nanoseconds to 100 μsec, in steps of 10 nanoseconds, to be introduced between the event and the beginning of the picture streak. The trigger into the trigger delay generator need only be a few volts in amplitude and have a rise rate greater than 1v per μsec. Using a fibre optic it is possible to use a light signal as trigger, because the TDG contains a photocell which will provide the required electrical trigger. The sensitivity of the TDG can be set using a calibrated attenuator both for an optical signal and an electrical signal.

5.6 Photomultiplier Power Supply.

The supply voltage to the photomultiplier tube is provided by a Fluke model 408B high voltage DC power supply capable of giving up to 20mA at 0 to ± 6000v. Line regulation is better than 0.001% for a 10% line change from nominal, and load regulation is better than 0.001% or 5mV (whichever is greater) for

full load change. Stability after warmup of 30 mins is ± 0.005% per hour and resetability is ± 0.05% or 50mV (whichever is greater). It can be shown that the fractional change in gain (G) of the photomultiplier tube is related to the fractional change in overall applied voltage (V) by

$$\frac{dG}{G} = 0.7n \frac{dV}{V} \qquad (5.6.1)$$

where n = number of dynodes = 14.

The ripple on the applied voltage is less than 5mV peak-to-peak giving a fractional change in gain of $< 3.10^{-6}$ for an applied voltage of 2KV (i.e. a percentage change of < 0.0003%).

5.7 The Photomultiplier.

The photomultiplier used in the experiments was an EMI tube type 9594 QUB capable of a pulse rise time of 2 nanoseconds. A fast linear focussed structure of 14 dynodes, coated with antimony caesium secondary emitting material, provides a gain in excess of 10^8, with an output current linear to above 300 mA with a suitable voltage distribution along the dynodes. A curved cathode of semitransparent S20 type (see fig. 5.8 for response curve) is deposited on a window which is flat externally. A system of focussing electrodes providing spherical equipotentials gives a spread in transit time of 2 nsec for photoelectrons from various

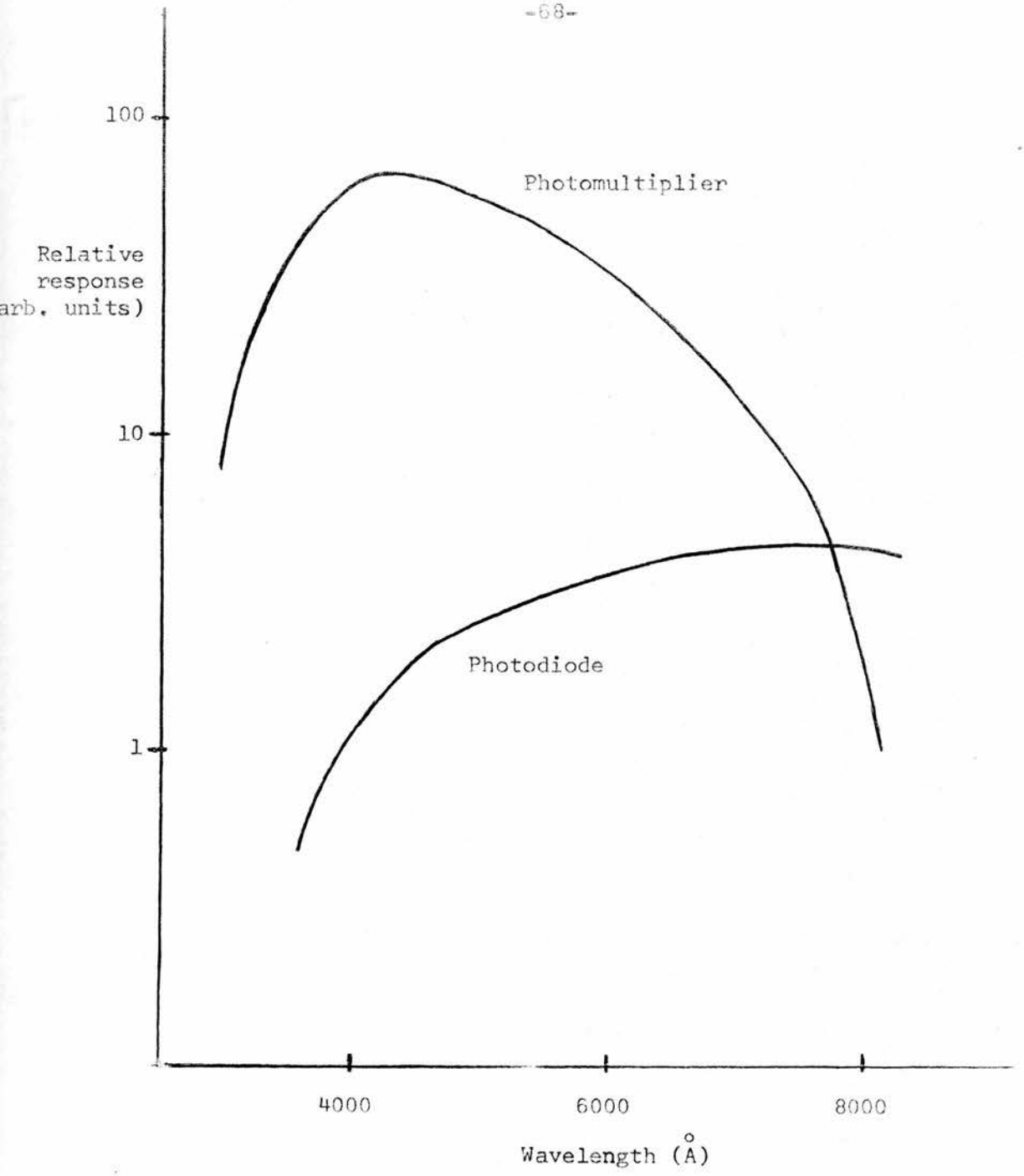

Fig. 5.8: Response curve of photomultiplier cathode and photodiode.

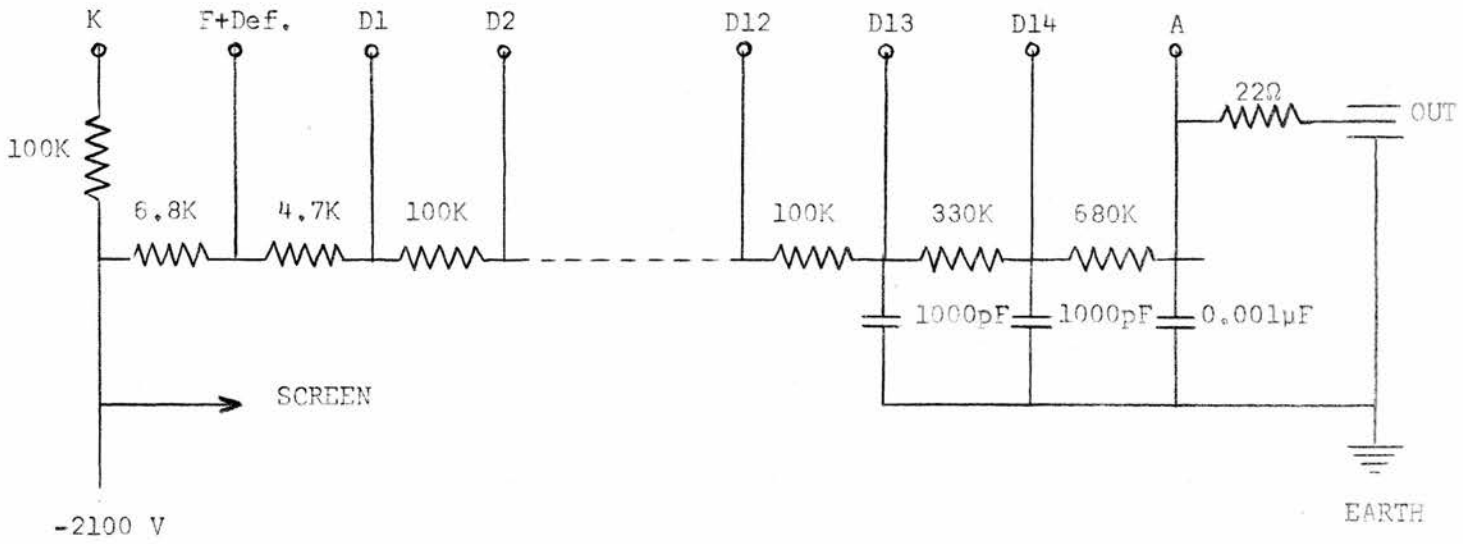

Fig. 5.9: Resistor chain and output circuit of photomultiplier.

parts of the cathode into the first dynode (D1). A deflector electrode optimises the time spread between D1 and D2.

The electrodes of the tube are held at prescribed voltages using a resistor chain of the type shown in fig. 5.9. The voltages between successive dynodes one to eleven are the same whereas the voltages on the final stages are progressively increased from D11 to D14 and the anode (A) to prevent loss of linearity due to space charge buildup. The voltages on the first stages including the deflector and focus electrodes must be set as recommended for the particular tube being used. Typical voltages are 160v between the cathode and deflector and 40v between the deflector and D1. The focussing electrode is tied to the same potential as the deflector electrode. The required overall voltage depends on the sensitivity of the tube which is typically 5000 amps per lumen at an overall voltage of 2.4KV.

Decoupling capacitors are necessary in the last stages to prevent variation of the dynode voltages when a signal is put into the tube. If an average anode current i_a flows then a charge $i_a t$ will be taken from the capacitor (C) decoupling D14 to the anode (t is the pulse duration). The voltage of D14 will vary by $\frac{i_a t}{C}$ giving a change in gain (see equation 5.6.1) of

$$\frac{dG}{G} = 0.7 \frac{i_a t}{CV_s} \qquad \text{where } V_s = \text{stage voltage.}$$

If linearity of L% is required then $100 \frac{dG}{G} < L$

$$\text{i.e.} \qquad C > \frac{70 i_a t}{LV_s} \qquad (5.6.2)$$

The output stage is designed to supply a signal into 50Ω cable terminated in 50Ω.

5.8 Photodiode.

The photodiode used to record the stimulated emission pulses was a Hewlett Packard pin photodiode type HP 4201 which has a speed of response of less than 1 nsec. Its spectral response in the region 4000 → 10,000 Å is shown in fig. 5.8. The active region of the photodiode is 0.020 inches in diameter and the HP 4201 incorporates a fibre optic light guide which places this region optically on the end surface of the device. Sensitivity is typically 0.3 μA/mW/cm^2 at 5000 Å and bias of 20v. The diode is incorporated in a simple circuit providing reverse bias and an output impedance of 50Ω to match 50Ω cable and load.

5.9 Oscilloscope.

The signals from the photodiode, photomultiplier, current probe and voltage divider were recorded on polaroid type 410

10,000 ASA film from the screen of a Tektronix type 555 double beam oscilloscope using two type L plug-in units. The type L plug-in amplifier incorporates a high gain calibrated dc amplifier plus a fast rise high gain ac amplifier with a band-pass of dc to 30mc/s. The L unit has a rise time of 6 nano-seconds alone or 12 nanoseconds when used with the 555 oscil-loscope and an input impedance of 1MΩ shunted by 20pF. Voltage sensitivity is from 5mV/cm to 20V/cm in eighteen calibrated steps with accuracy of within 3% for all positions. A cali-bration square wave output is provided in the 555. Sweep rates are from 0.1 μsec to 5 seconds per centimetre in 24 calibrated steps with an accuracy to within 3% of scale setting. Trigger-ing is provided from the input signal of either input with both a positive or negative slope facility and ac or dc coupling.

Single sweep mode can be used for photographing an input waveform that varies in amplitude or shape. On pushing a button on the instrument the oscilloscope will trigger and sweep once on the first available signal and then stop. This facility is used when obtaining variation of spontaneous emission with current, say, when the spontaneous emission pulse corresponding to a particular current pulse can be photographed.

5.10 Monochromator.

The monochromator used was a Grubb Parsons instrument type

M2 with a grating blazed for 1st order, and having 15,000 lines per inch. At small slit apertures this enabled resolution between lines about 2 Å apart, and this was sufficient for most of the region of interest. A section of the discharge tube was imaged on the input slit by an f/2 lens and screens were set up inside the instrument to prevent scattered light reaching the output slit. The instrument was aligned using a He-Ne laser and calibrated using a mercury lamp. The resultant scale measurements in the region of 4000 Å were fitted to a straight line using a least squares method and from this unknown lines were identified. References to the relative intensities published by Rudko and Tang (21) also helped in identification of the lines.

CHAPTER VI - STREAK PHOTOGRAPHY RESULTS

6.1 Introduction.

The apparatus arrangement for these experiments is shown in fig. 6.1. The streak camera is positioned to photograph a dispersed image of the stimulated emission output of the laser, consisting mainly of the wavelengths 5145, 4965, 4880, 4765 Å. These images were formed by focussing the output of the laser onto a ground glass screen, after it had been dispersed by a diffraction grating. The camera was triggered to start the streak by a pulse from the thyratron of the laser power supply. This pulse was first shaped and delayed by the trigger delay generator, before reaching the camera. The resultant photograph was a time record of the development of the oscillation. A typical photograph, with three individual streaks on it, is shown in fig. 6.2. There was a jitter of about 1 μsec in the breakdown of the tube relative to the pulse from the thyratron, but this was permissible at a streak speed of 1 μsec cm^{-1}. Several streak photographs were taken under a given set of conditions, and the results were averaged to give the relevant information.

6.2 Stimulated emission delays.

The 4880 Å line was found to oscillate first under all conditions of the experiment, so the delays of the other lines

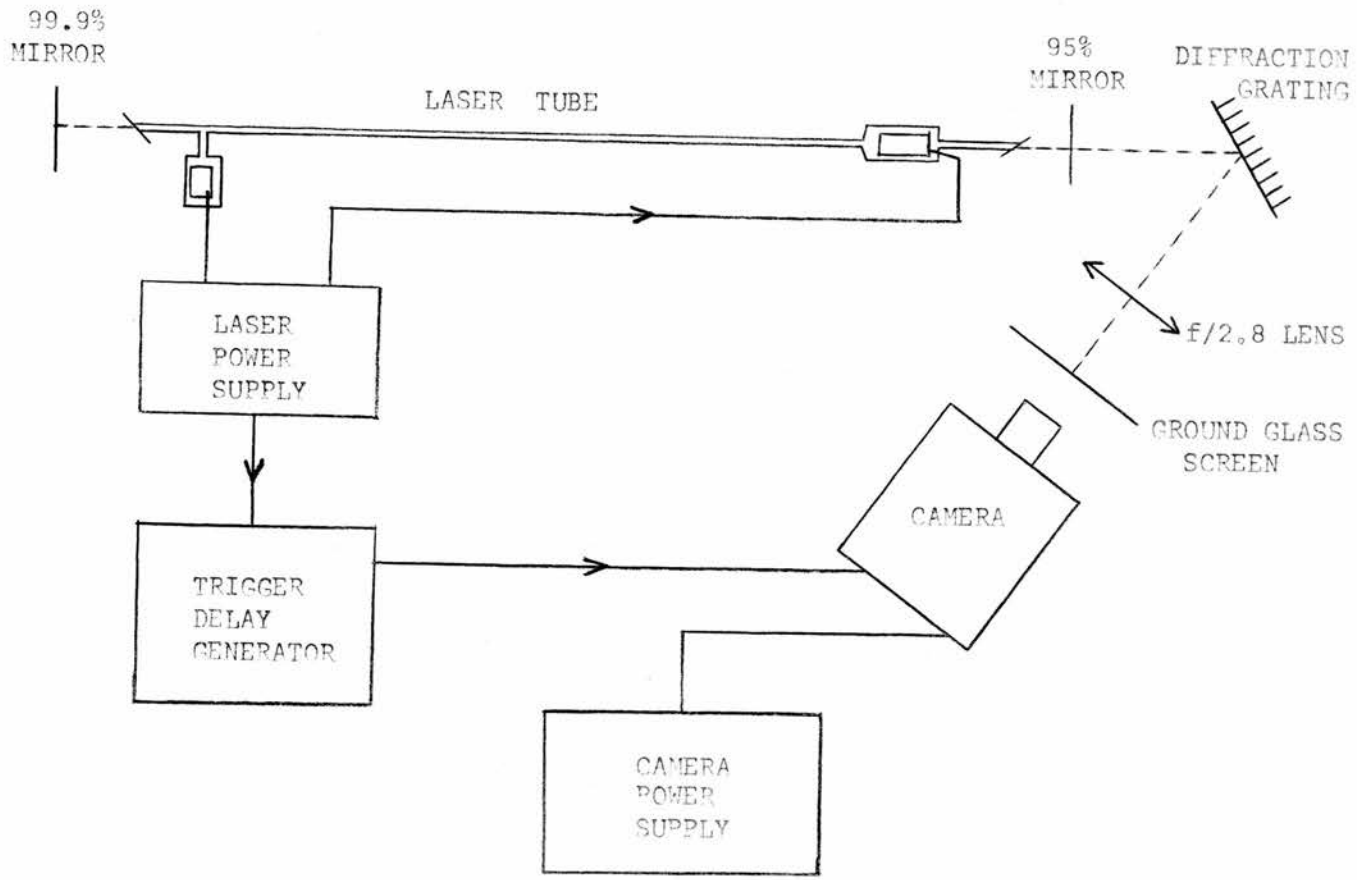

Fig. 6.1: Arrangement of apparatus for streak photography.

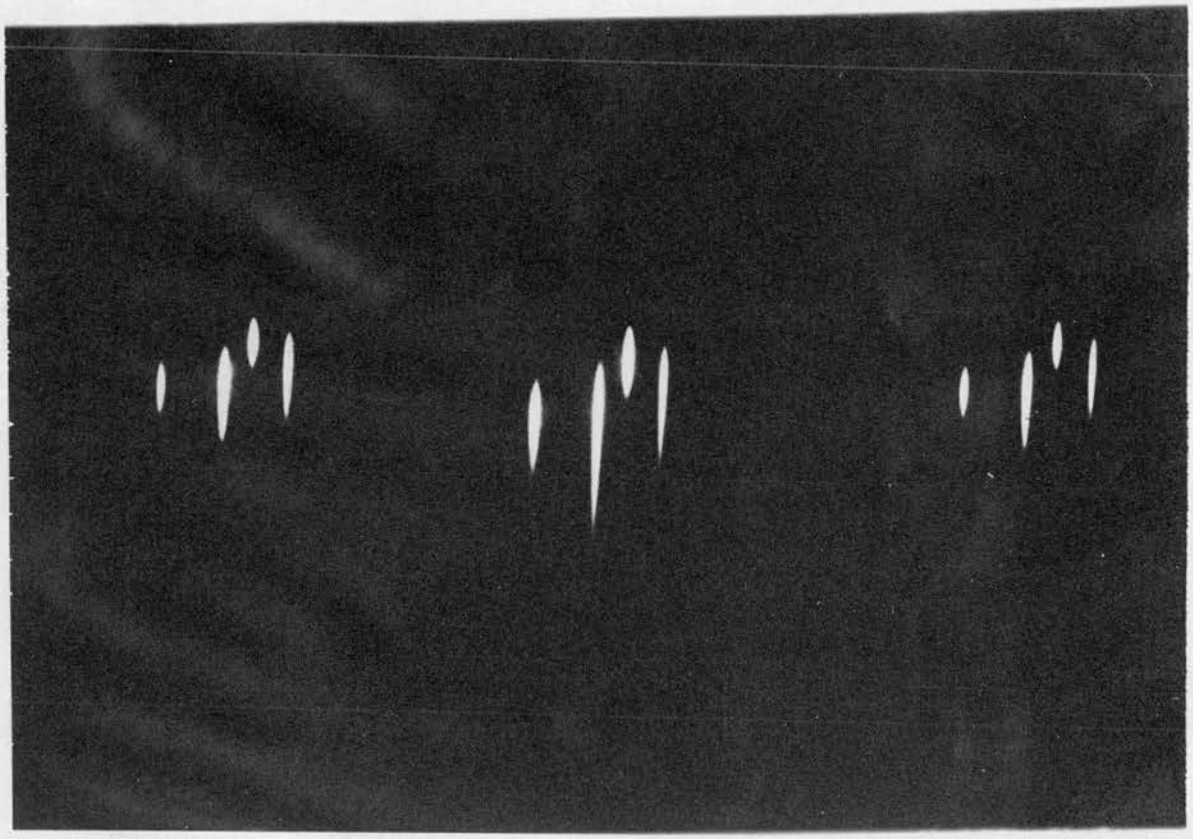

Fig. 6.2: Typical streak photograph for three pulses. From left to right lines in a group are 5145 Å, 4965 Å, 4880 Å and 4754 Å. [1 μsec. cm^{-1} streak speed].

were measured relative to the start of the 4880 Å stimulated emission. The variation of these delays with pressure and current density is shown in figs. 6.3, 6.4 and 6.5.

If the highest gain transition oscillates first then the order would be 4765 Å, 4880 Å, 4965 Å, 5145 Å (see fig. 4.2) but it was found that the order was in fact always 4880 Å, 4765 Å, 4965 Å, 5145 Å. The threshold gain of the 4765 Å line is about 3.7 db/m and that of the 4880 Å line is about 3 db/m. However the mirrors forming the cavity have a peak reflectivity (95%) at 4880 Å and a reduced reflectivity (94%) at 4765 Å so that an extra loss is introduced at 4765 Å. It has been shown by Rigrod (51) that the output intensity (ω_t) of a high gain laser can be written

$$\frac{\omega_t}{\omega_o} = \frac{t}{a + t} \left[g_o \ell + \ell n(r)^{\frac{1}{2}} \right] \qquad (6.2.1)$$

where ω_o = saturation parameter

t = transmission of mirror

a = loss in mirror

r = reflectivity of mirror

g_o = unsaturated gain

ℓ = length of the laser .

This assumes that one mirror is completely reflecting and lossless.

At threshold ($\omega_t \equiv 0$) from (6.2.1)

$$g_o \ell = - \ell n(r)^{\frac{1}{2}} \qquad (6.2.2)$$

It is then possible to show by differentiation of (6.2.2) that any decrease in the reflectivity is equivalent to reducing the threshold gain by a certain amount (e.g. changing the reflectivity from 0.95 → 0.94 is equivalent to reducing the gain by 25%). Thus the effective gain at 4765 Å will be reduced due to the spectral response of the mirrors.

From figs. 6.3 and 6.4 it can be seen that the delays between the lines are relatively constant at current densities of 4400 Acm^{-2} but that considerable variation occurs at about 2600 Acm^{-2}. In particular it is found that the delays of the 4965 Å and 4765 Å lines are becoming larger at higher pressures when the current density is about 2600 Acm^{-2}. Higher pressure means a lower electron temperature and a greater collision frequency.

From the results of Sobolev et al (48) it is possible to extrapolate into the region of 50 mtorr to find the electron temperature as a function of current density. This is shown in fig. 6.5 from which it can be shown that an increase in pressure from 50 → 60 mtorr reduces the electron temperature by about 1%. This would be unlikely to cause significant change in the multistep mechanisms. However the cross section for single

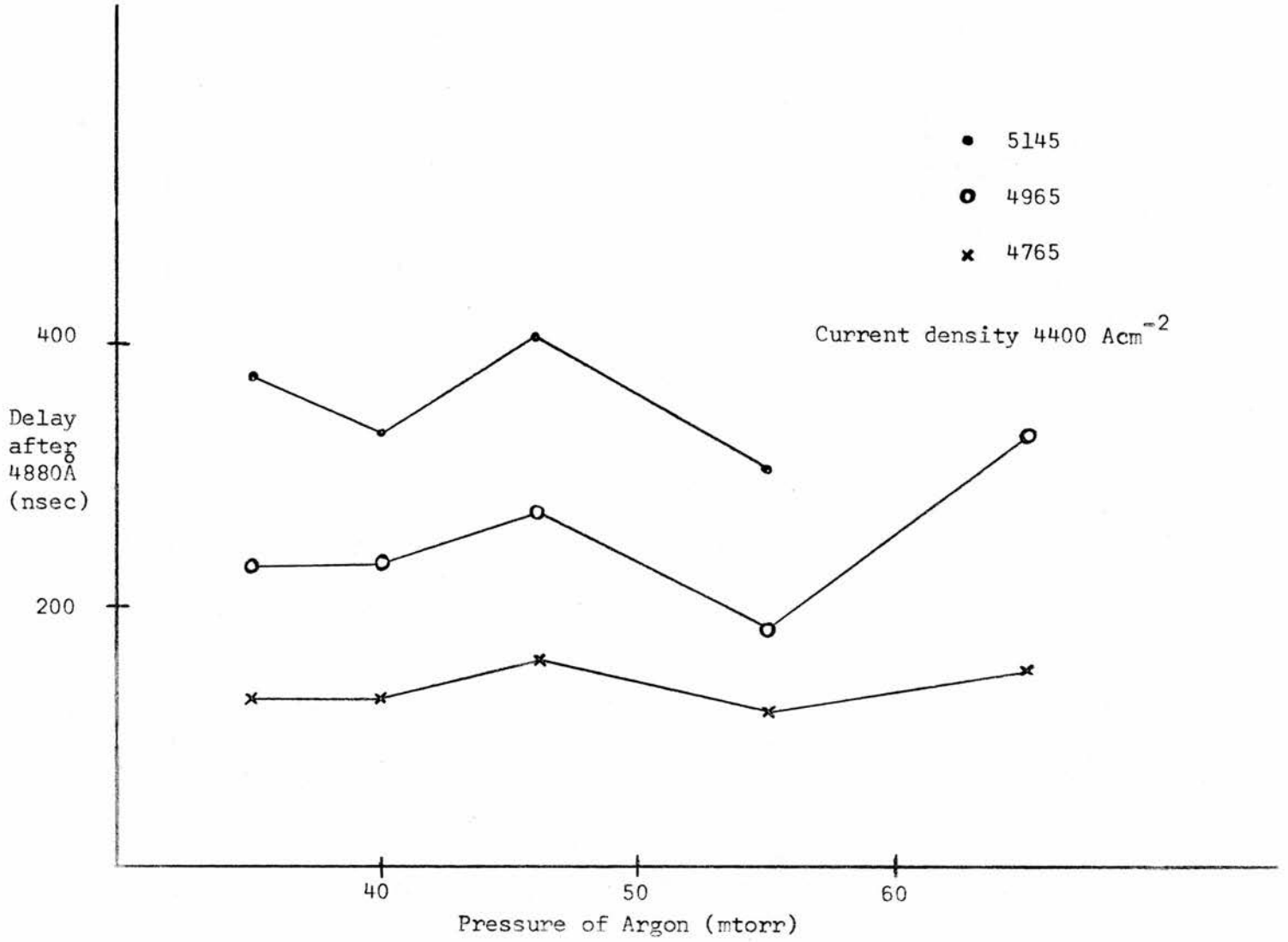

Fig. 6.3: Variation of delays with pressure.

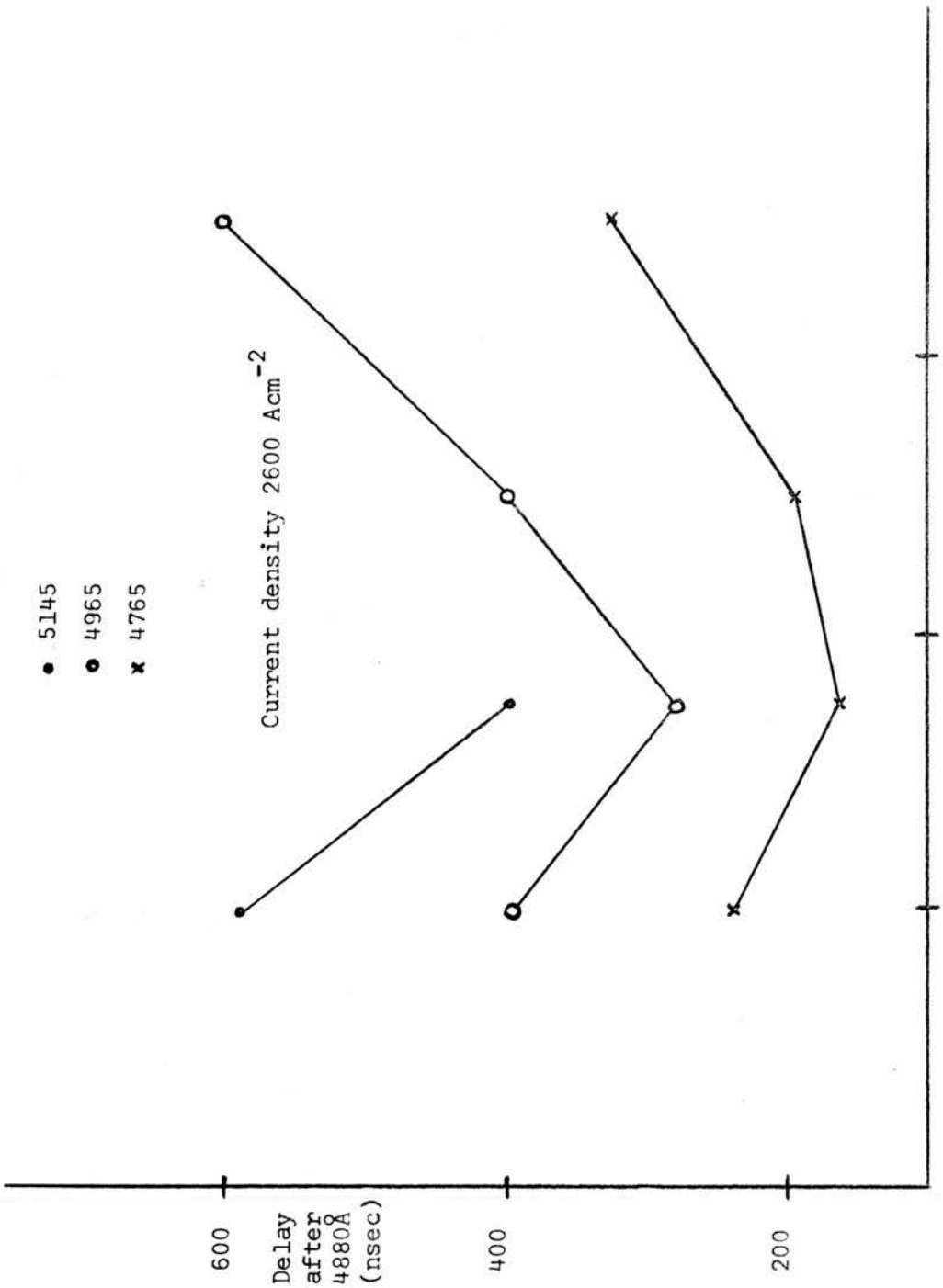

Fig. 6.4: Variation of delays with pressure.

step excitation as measured by Bennett (31) [see fig. 6.6] varies rapidly with electron temperature near threshold and a 1% reduction in electron temperature causes about 15% reduction in a single step process. These considerations suggest that threshold for a single step process occurs at about 2600 Acm^{-2}. From the results of Sobolev et al (48) it can be seen that this current density would be equivalent to an electron energy of about 40 eV which corresponds roughly to the measured threshold energies for single step excitation by Bennett(31). It will be shown later in section 7.2 that the advent of a single step process is sufficient to explain the observed saturation behaviour of the spontaneous emission at a current density of about 2600 Acm^{-2}.

Fig. 6.7 shows the variation of the delays with current density at a fixed pressure. The current scale is actually equivalent to an electron temperature scale so that at low electron temperature the delays are long but decrease rapidly until about 2600 Acm^{-2} when there is a gradual decrease as the electron temperature rises. This can be explained on the same basis as the previous results and again indicates that the threshold for the single step process is in the region of 2600 Acm^{-2}. Above threshold the cross section is fairly constant (31) and so one would expect a flattening out of the curves.

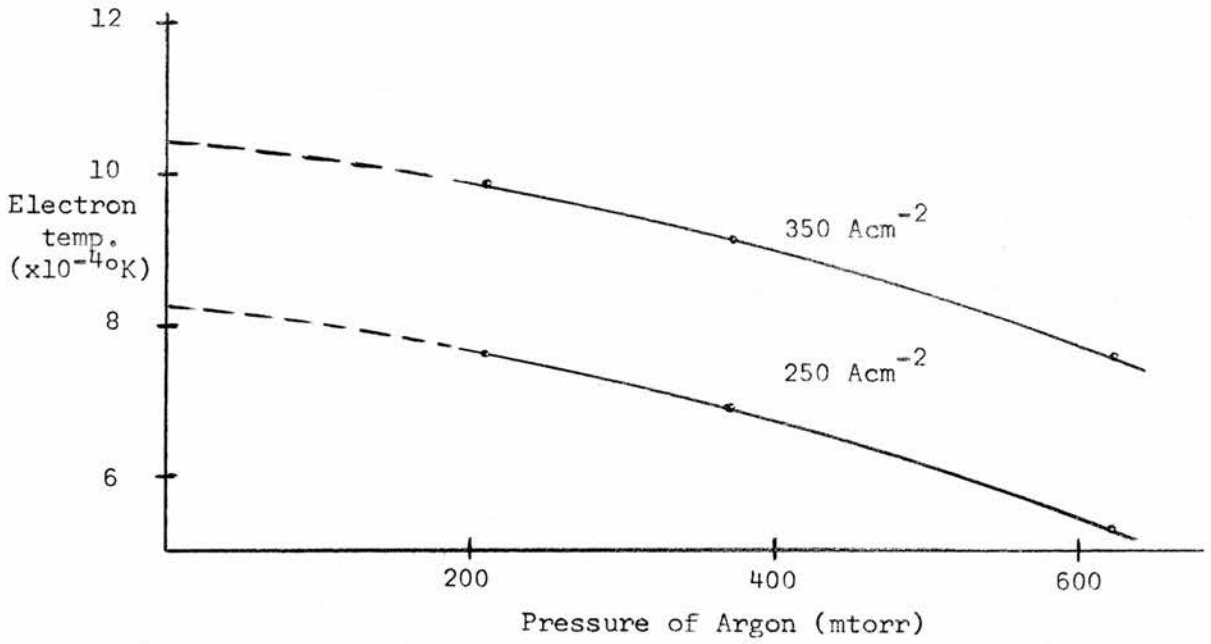

Fig. 6.5: Variation of electron temperature with pressure.

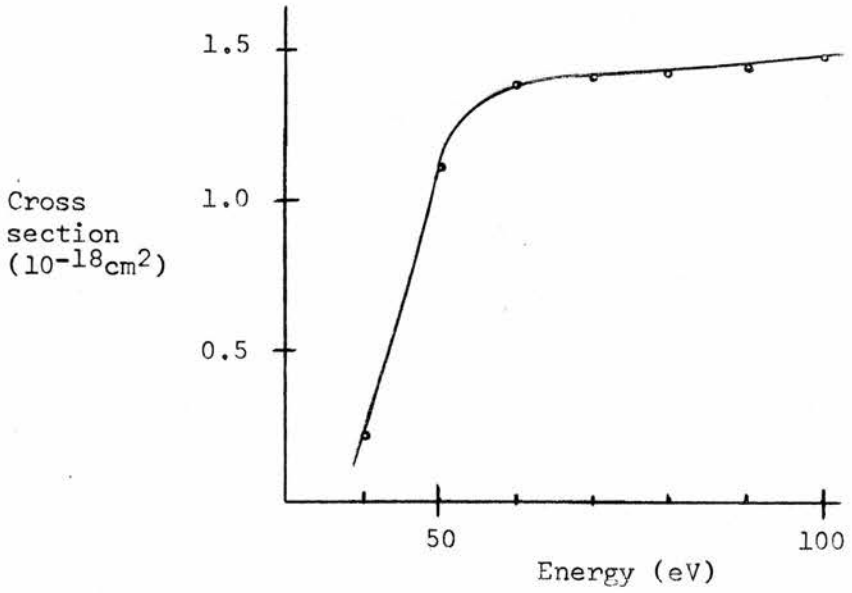

Fig. 6.6: Variation of single step mechanism cross section with energy.

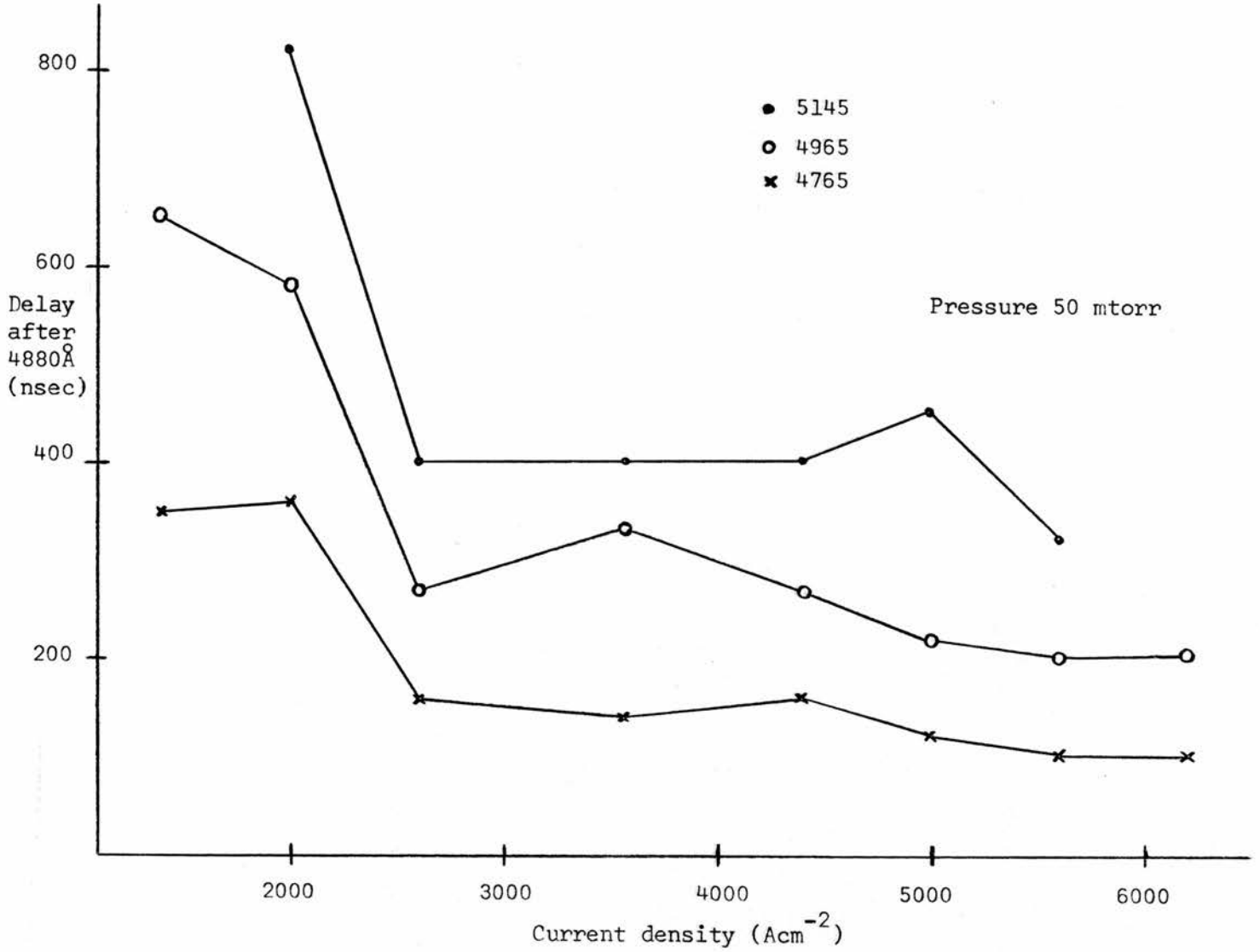

Fig. 6.7: Variation of delays with current density.

6.3 Duration of the stimulated emission pulses.

The length of the streak (i.e. the time for which the gain exceeds the losses on a transition) was measured as a function of the current density at 46 mtorr (fig. 6.8), and as a function of pressure at a current density of 4400 Acm^{-2} (fig. 6.9). There is a maximum in the streak length at a pressure of 40 mtorr and a current density of 2600 Acm^{-2}. Since the delay to the initiation of the pulse is almost constant at 50 mtorr and above 2600 Acm^{-2} (fig. 6.7), then fig. 6.8 effectively shows the time after the initiation of the 4880 Å line when the gain on each transition becomes less than the losses (i.e. when the oscillation ceases). Two processes can cause a cessation of the oscillation 1) the pumping to the upper level of the transition decreases or 2) the lower level population increases. Both mechanisms will destroy the population inversion. It will be shown (section 7.5) that the upper level is still being populated when the oscillation ceases , thus implying that this is a lower level effect.

It is also apparent that the four wavelengths divide into two groups with the 4880 and 5145 Å lines behaving similarly and the 4965 and 4765 Å lines behaving similarly. The former pair have a common lower energy level at $(^3P)\ 4s\ ^2P_{3/2}$ and the latter pair have a common lower energy level at $(^3P)\ 4s\ ^2P_{1/2}$.

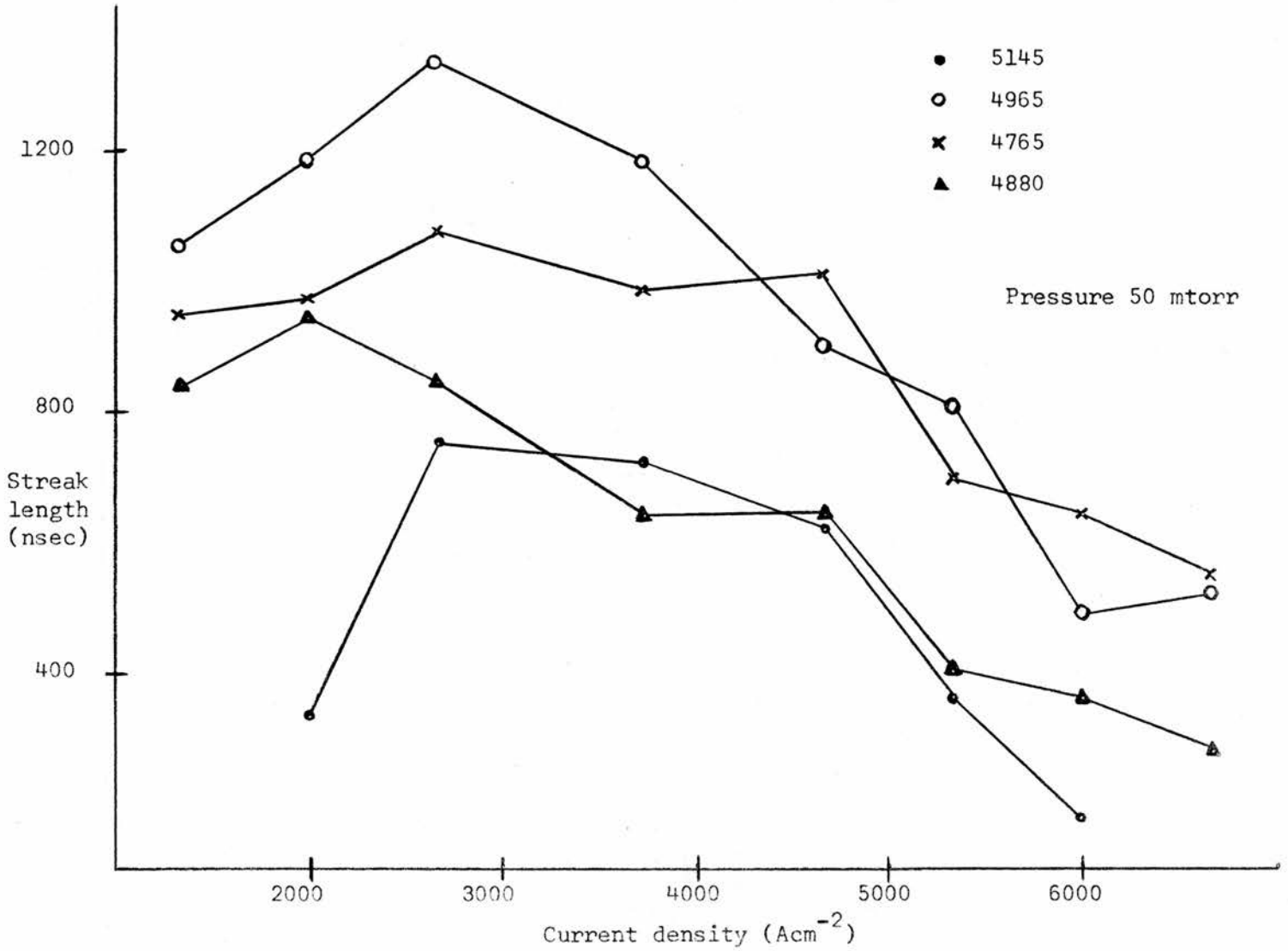

Fig. 6.8: Variation of streak length with current density.

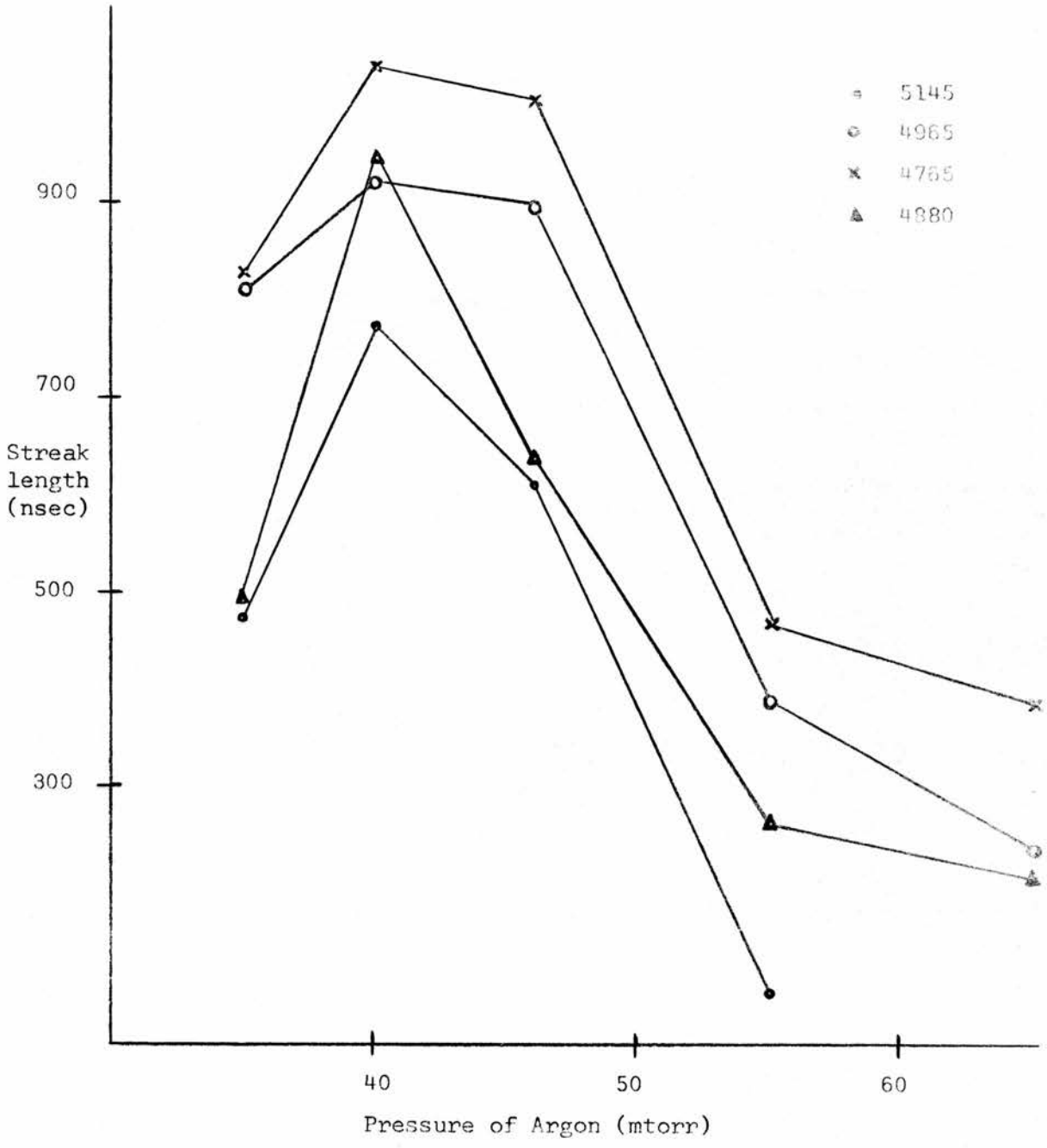

Fig. 6.9: Variation of streak length with pressure.

Since the upper levels all have a similar energy, it might be expected that the lines would group as they do if the lower level is having some effect on the shortening of the pulse length. The pulse length begins to decrease at current densities above about 3000 Acm^{-2}. Cheo and Cooper (45) showed that radiation trapping in the argon ion laser at 10 mtorr and current densities of 8000 Acm^{-2} was a significant process. Reference to their fig. 2 of the current and pressure conditions to attain radiation trapping, shows that at 50 mtorr pressure one would expect radiation trapping at a current of 700 amps through a 5 mm bore tube. This corresponds to a current density of about 3500 Acm^{-2}. Thus above this current density the lower laser levels in the 4s ion states would be increased in lifetime causing less inversion and the lasing action would be quenched. It would also be expected that transitions to the same lower level would behave similarly.

At current densities below 2600 Acm^{-2} the streak length again decreases; radiation trapping effects are no longer applicable, but it is possible that the rapid decrease of the importance of the single step pumping mechanism, which was noticed in section 6.2, is causing a decrease of the upper state population and is leading to reduced streak length. Again the indicated point for the start of this process is at a current density of 2600 Acm^{-2}.

Fig. 6.6 shows that the streak length decreases as the pressure increases and this is compatible with both increased importance of the radiation trapping process and decrease of the electron temperature. The grouping of the lines as discussed above is still noticeable but is not so marked. Cheo and Cooper (45) showed that increased radiation trapping would occur at higher pressure. This would be expected since the density of atoms in the ion ground state would be greater, causing greater trapping between the 3p ion ground state and the 4s states. The decrease of the streak length as the pressure decreases can be explained by the fact that the collision frequency will be decreasing with pressure. The collision frequency is roughly proportional to the pressure so a decrease in pressure from 40 → 35 mtorr causes about 10% decrease in the collision frequency with subsequent reduced pumping.

CHAPTER VII - TIME RESOLVED SPONTANEOUS AND STIMULATED EMISSION

7.1 Introduction.

The experimental apparatus was arranged as shown in fig. 7.1 for this part of the investigation. The sidelight or spontaneous emission coming from the tube transverse to its axis was focussed into the slit of the monochromator and the output of the monochromator was converted by a photomultiplier into an electrical signal which was displayed on an oscilloscope. The stimulated emission was detected by a photodiode as described in (section 5.8) and the current measured by a current probe (section 5.4). The oscilloscope was dual beam so two out of these three signals could be displayed together and photographed.

The intensity of the spontaneous emission as a function of current was plotted for several selected transitions including transitions of the type $5s \rightarrow 4p$, $4d \rightarrow 4p$, $4p \rightarrow 4s$ and $4p \rightarrow 3d$. All these transitions showed the same behaviour similar to that shown in fig. 7.2. At current densities below about 1800 Acm^{-2} the curves all showed a quadratic dependence of spontaneous emission on current density, whereas in the region above 1800 Acm^{-2} the spontaneous emission showed a saturation behaviour, becoming linear with current density and then almost independent of current density. The curves were obtained by keeping the applied voltage constant and varying a non-inductive resistor in

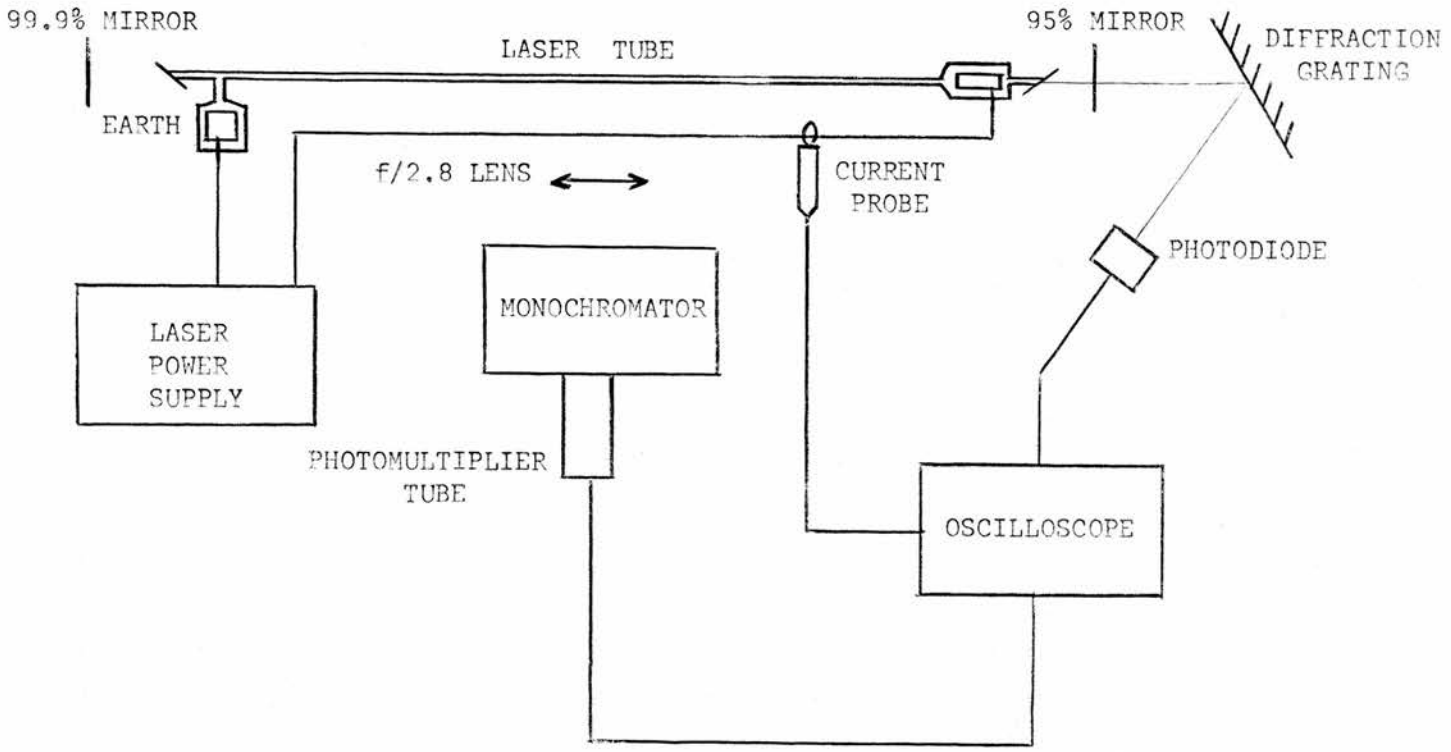

Fig. 7.1: Arrangement of apparatus for spontaneous emission measurements.

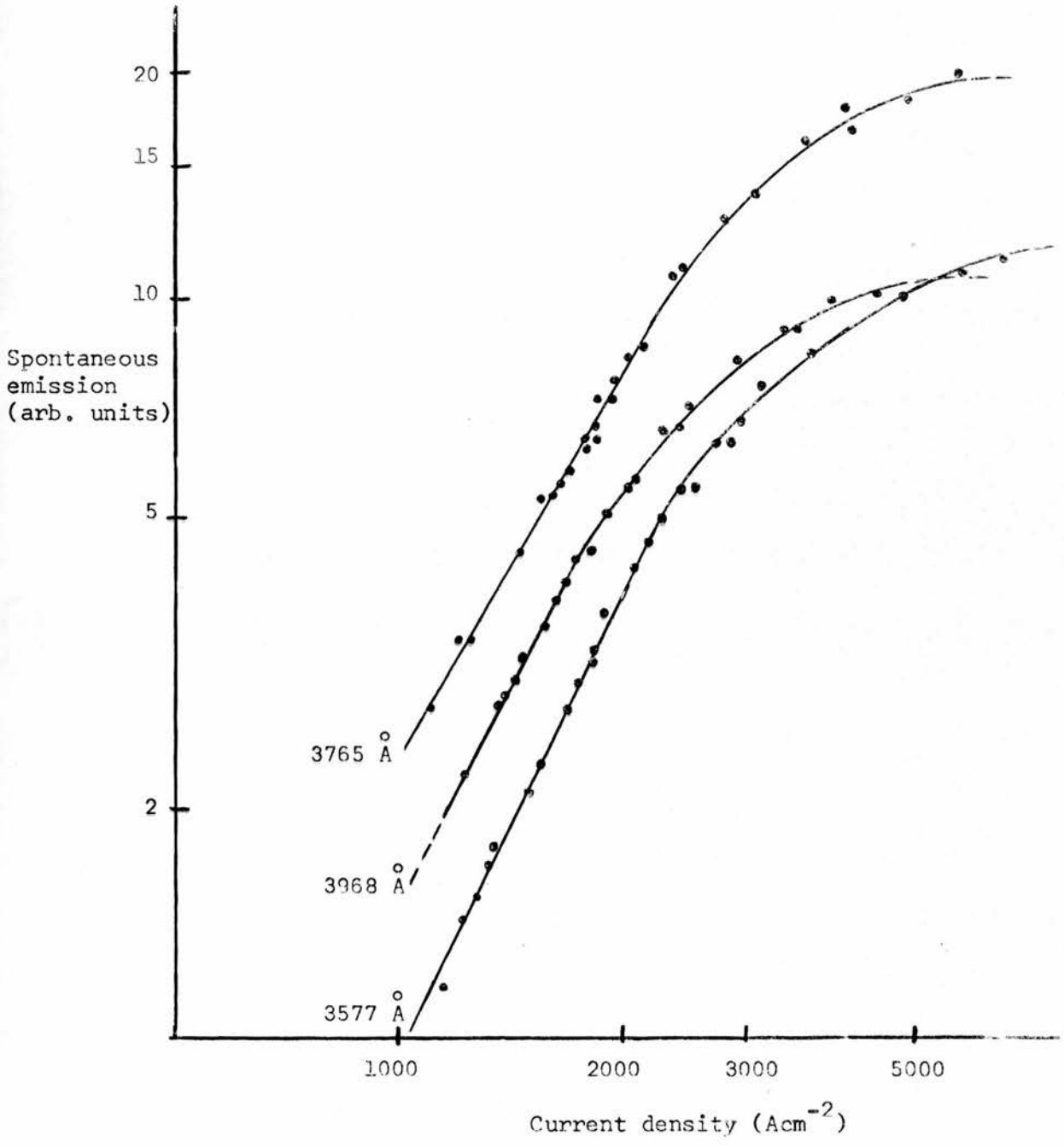

Fig. 7.2: Relative spontaneous emission intensity as a function of current density.

series with the laser discharge tube. This ensured that the breakdown voltage was the same for each point of the curve. Typical traces shown in fig. 7.3 are for different values of the current density (1) with the spontaneous emission at 4765 Å. Fig. [7.3(a)] is for a peak current density of 5000 Acm^{-2} and fig. [7.3(b)] for a peak current density of 1500 Acm^{-2}. It can be seen that for large current densities the peak of the spontaneous emission occurs before that of the current density and vice versa for lower current densities. The explanation of this lies in the saturation behaviour of the spontaneous emission. When the current reaches a certain value further increase of the spontaneous emission is impeded and the decay of the spontaneous emission will be determined by the dominant deexcitation mechanism of the upper level and its relation to the excitation caused by the current.

At lower current densities and thus lower electron densities the spontaneous emission does not saturate and the very slight delay of the peak of the spontaneous emission after the peak of the current pulse can be explained by the slight decay between the excitation and its appearance in the spontaneous emission. Note that the initiation of spontaneous emission is slightly delayed in both cases by a similar amount of about 100 nsec.

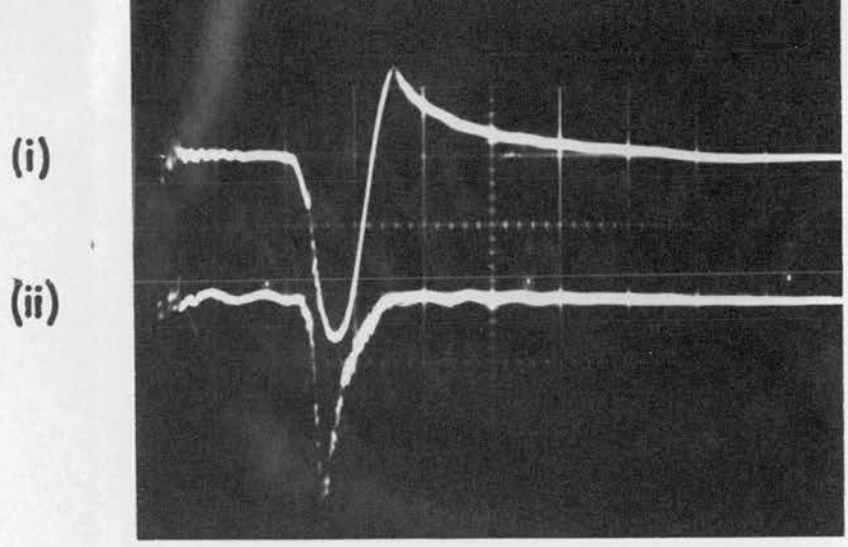

Peak current 5000 Acm^{-2}

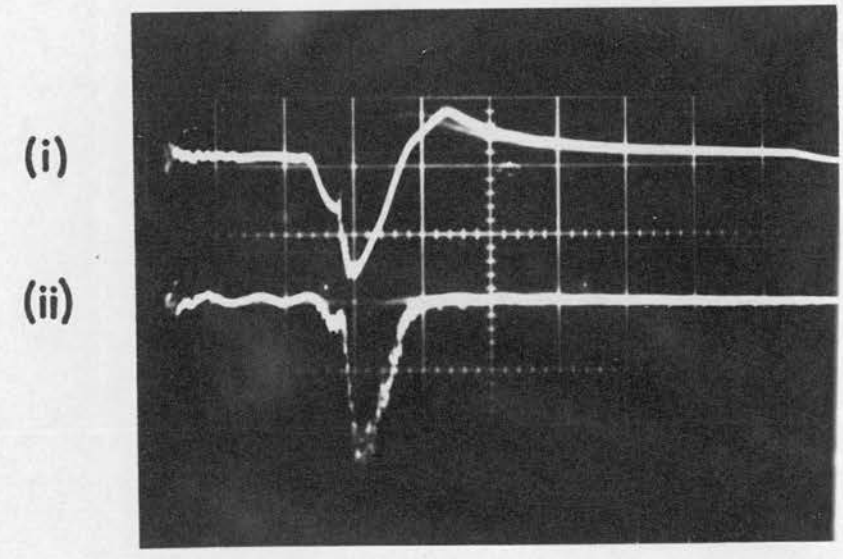

Peak current 1500 Acm^{-2}

Fig. 7.3: Time resolved (i) current (ii) spontaneous emission pulses [2 μsec/cm, 40 mtorr Argon].

The behaviour of about 20 transitions was investigated in this way and from the photographs the time resolved intensity of the spontaneous emission gave information on the behaviour of the upper level population for each transition. This enabled correlations of the stimulated emission output from the upper laser levels with the spontaneous emission output and with the cascade contributions from the 5s and 4d levels into the 4p levels.

7.2 Saturation of Spontaneous Emission.

The explanation of the saturation behaviour observed in the spontaneous emission at current densities of > 2000 Acm^{-2} can be found in either the collisional effects of the electrons on the 4p → 4s transition or in the excitation mechanism from the ground states or possibly a combination of both. The large effect of electron collision on the 4p → 4s ion transitions has been discussed in section 4.6 to some extent. Recent calculation of the electron-ion collision cross sections by Beigman et al (38) have shown that at electron densities of about 10^{15} cm^{-3} the deactivation rate for the 4p → 4s ion transitions would be about 8.10^{8} sec^{-1}. This is an order of magnitude greater than the radiative decay, and so would be expected to be the dominant decay mechanism. Similarly,

excitation from the 4s metastable states would be significant. It was shown in section 4.6 that this would lead to a population in the 4p states which would be linearly dependent on current density. Therefore the spontaneous emission, which depends only on the upper level population, would become linearly dependent on current density. A similar argument holds for the 5s and 4d states. It is possible to make extrapolations from the measured dependence of electron density on current density by Kitaeva et al (6) to find the current density which would correspond to an electron density of 10^{15} cm^{-3}, when the collision process would be appreciable. This indicates a current density of 2500 Acm^{-2}, so we would expect this process to be significant at about the same current densities that give saturation as in fig. 7.2.

It has been shown in section 4.2 that there is considerable evidence that a single step process becomes a significant pumping mechanism whenever the electron energy exceeds about 40 eV. From the results of Kitaeva et al (48) this energy is found at a current density of 2500 Acm^{-2}. The single step process would give a contribution to the pumping of the upper levels which would depend linearly on current density, and so the observed quadratic dependence would gradually change to a linear dependence when the single step process was appreciable.

This observed behaviour agrees favourably with the results of section 6.2.

The complete saturation of the spontaneous emission would occur in this model if the ground state of the atom becomes seriously depleted due to the ionisation process. It can be simply calculated that the density of atoms in the laser at the pressure and atom temperature in the discharge would be about 4.10^{15} cm^{-3}. Appreciable ionisation of these atoms would give an electron density of about 3.10^{15} cm^{-3} which would occur at a current density of about 5500 Acm^{-3}. This assumes that the linear dependence of electron density on current density is maintained into the region of interest. Depletion of the atom ground state population is thus going to hinder the excitation process and cause the population of the upper levels of the spontaneous emission to become independent of current density.

7.3 Relation of saturation to upper level energy.

If the current density at which the gradient of the curves obtained for the variation of spontaneous emission intensity becomes unity, is plotted against the upper level energy for the transition involved, it is found that the transitions from the 4p levels saturate before the transitions from the 5s and

4d levels (see fig. 7.4). The general trend is that transitions with the lowest upper level energy saturate first. The transitions from the 4p states saturate at about 2400 Acm^{-2} with the transitions from the 4d and 5s states saturating at about 3000 Acm^{-2}.

The 4p → 4s and 4p → 3d transitions have a higher cross section for electron deactivation than do the 5s → 4p and 4d → 4p transitions (38). This means that electron collision becomes significant on the 4p levels before the higher energy levels and we would expect a grouping of the 4p levels at a lower current density than the corresponding 4d and 5s levels.

On the basis of a single step excitation it can be shown that the 5p ion levels have a smaller probability of being excited (28) and that it is not possible to excite the 5s and 4d levels directly in a single step excitation from the argon atom ground state, because of the selection rules. The 5s and 4d levels therefore depend on cascade from the 5p levels for their single step contribution to their population. It would be expected then, that a higher electron energy, and thus current density, would be necessary to produce a population in the 4d and 5s levels which would depend linearly on current density, by virtue of the single step contribution to its population.

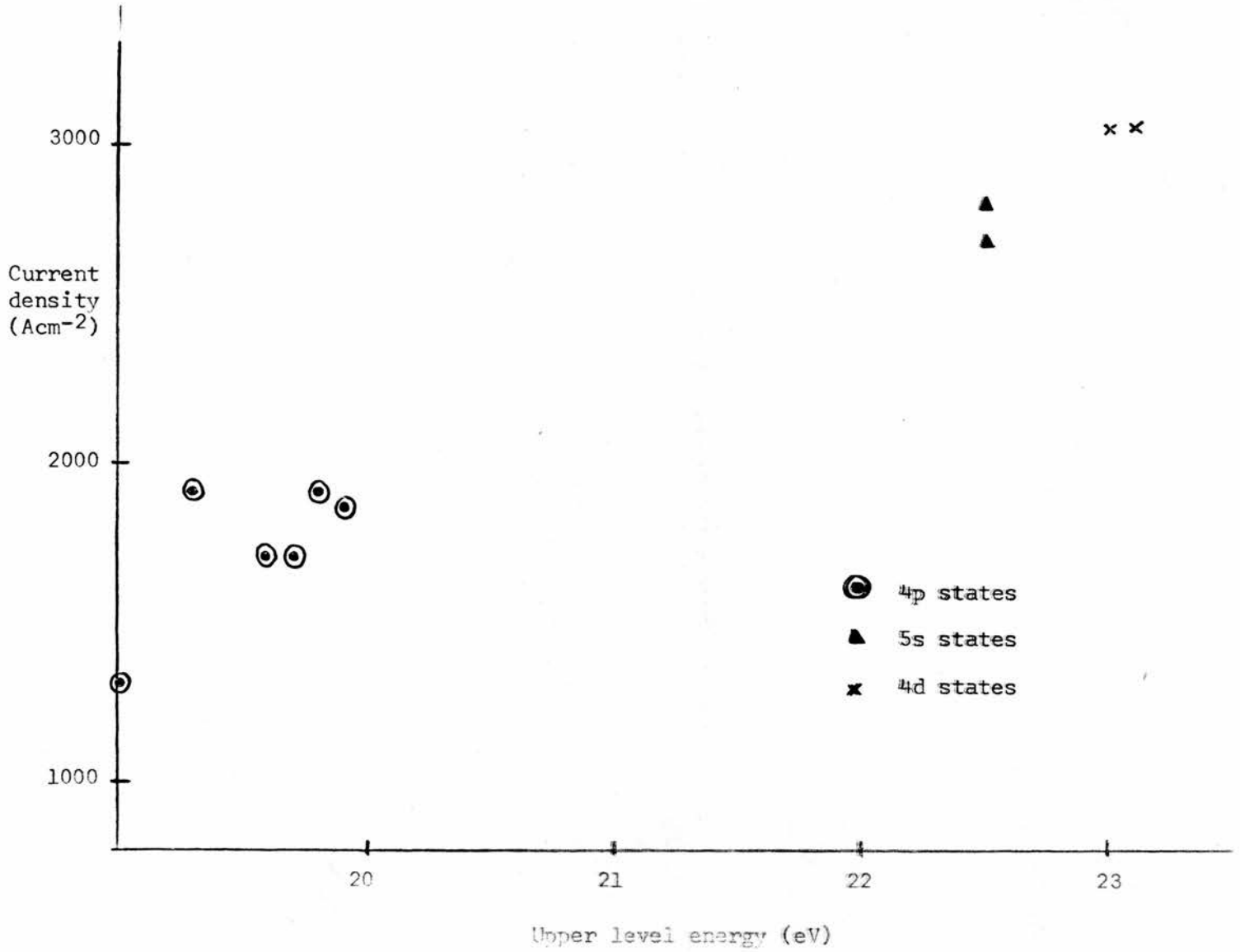

Fig. 7.4: Variation of saturation current with upper level energy.

7.4 Relation between spontaneous emission and stimulated emission.

It can be shown from Lamb's Theory of the Optical Maser (52) that the amplitude E_n of the stimulated emission radiation is related to the population ($\bar{N}$) of the upper laser level by the equation

$$E_n^2 = \frac{2\hbar^2 \gamma_a \gamma_b}{P^2} \left[\left(\frac{\pi^{\frac{1}{2}} P^2 Q_n \bar{N}}{h\varepsilon_o Ku} \right)^2 - 1 \right] \qquad (7.4.1)$$

where γ_a, γ_b = decay constants of upper level (a) and lower level (b)

P = electric dipole moment for the transition $a \rightarrow b$

Q_n = cavity quality factor for the nth mode

Ku = Doppler width of the ionic transition

$\hbar$ = $\frac{h}{2\pi}$ where h is Planck's constant

ε_o = permittivity of free space.

The above relation is obtained by substituting the expression for the quadrature component of the polarisation [see eqn.(79)] into the self-consistency equation (14) and rearranging terms. The expression applies for an inhomogeneously broadened line with a single mode at line centre in a standing wave approximation. This is equivalent to saying that the mirror losses should be small so that the waves travelling in the cavity

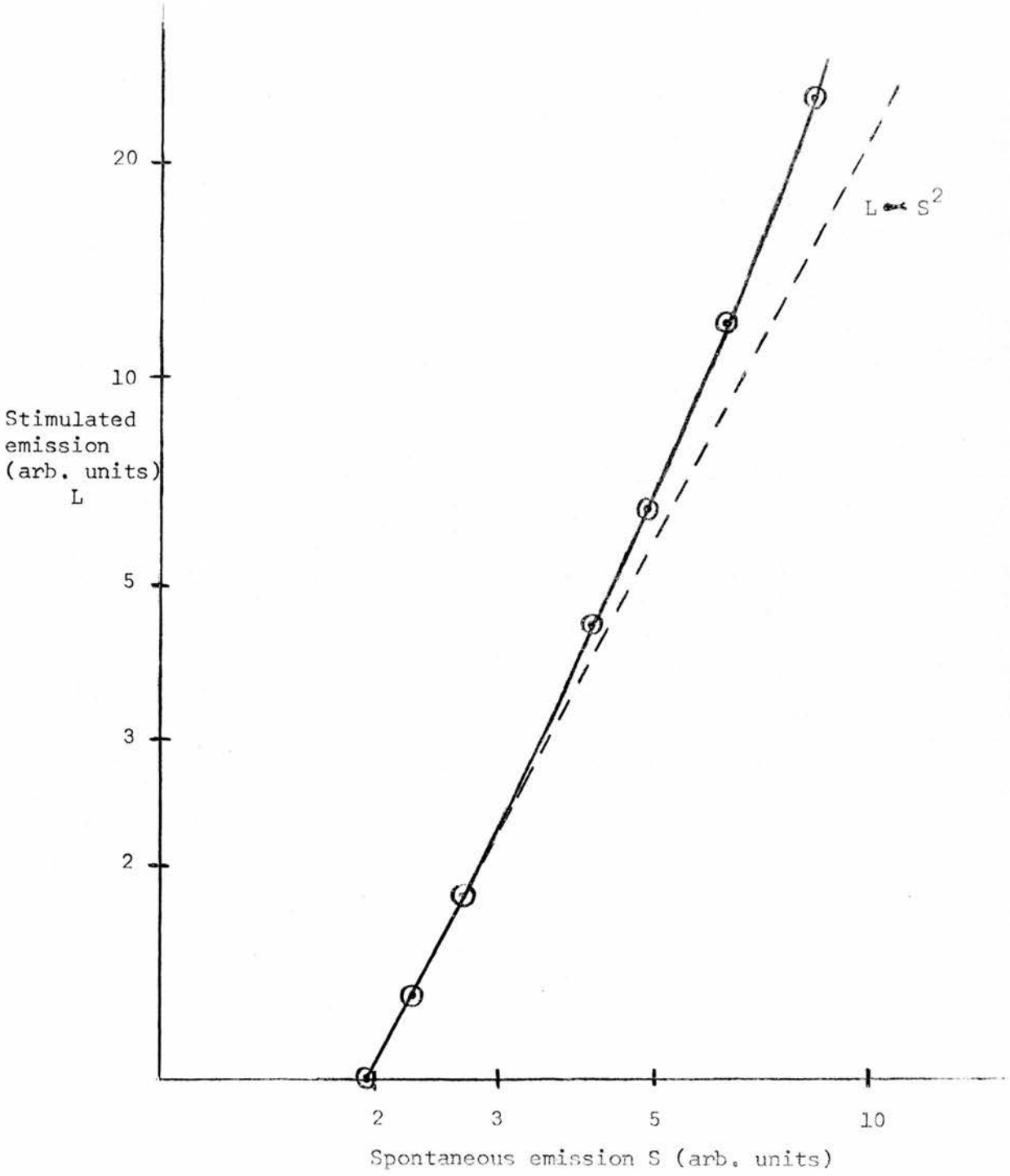

Fig. 7.5: Stimulated emission as a function of spontaneous emission.

combine to give a standing wave pattern with very little travelling component. The present work satisfies these conditions apart from the single mode criterion. The equations are taken to fifth order and should satisfy strong signal conditions as well as weak signal conditions.

Equation (7.4.1) can be simplified by collecting the constant quantities P, Q_n, $\bar{n}$ and ε_o and noting that the square of the amplitude E_n is just the stimulated emission intensity L, and that the population $\bar{N}$ will be directly proportional to the spontaneous emission intensity S, then (7.4.1) reduces to

$$L \propto \frac{\gamma_a \gamma_b}{Ku} S^2 \qquad (7.4.2)$$

The stimulated emission was plotted as a function of spontaneous emission as shown in fig. 7.5. For low intensities (i.e. low current densities) the curve follows a quadratic law with a calculated gradient of 1.95 but for higher currents, above 2300 Acm^{-2}, the gradient changes to a power greater than quadratic. This implies that the other quantities in equation (7.4.2) have changed [i.e. that the lifetimes of the upper or lower states have been shortened or the Doppler width has decreased]. It is unlikely that the Doppler width will have decreased since the gas will be increasing in temperature during the pulse and this leads to an increased Doppler width (see equation 2.2.7).

Also the lower level lifetime would be likely to increase by radiation trapping effects (see section 4.5) so that the upper level lifetime must have decreased in some way. A possible explanation for this is that the effect of collisional deexcitation on the 4p levels has shortened their lifetime causing γ_a to increase. Note that the onset of this effect is at about 2300 Acm^{-2} which corresponds to the values implied from the previous measurements (section 7.2) for the onset of the collisional deexcitation.

7.5 Evidence for Radiation Trapping.

The stimulated emission and the spontaneous emission for a particular transition were monitored together, and it was found that the stimulated emission saturated and decreased before the spontaneous emission had reached its peak value. The stimulated emission depends on both the upper and lower level lifetimes, whereas the spontaneous emission depends only on the upper level lifetime so this effect was interpreted as some lower level effect. This is most probably a radiation trapping effect caused by the reabsorption of the vacuum ultraviolet emission along the length of the tube (see section 4.5) which destroys the short lifetimes of the 4s lower laser transition states. Evidence for a lower level radiation trapping effect was also found in section 6.3. The cascade pumping

of the 4p states from the 4d and 5s ion states were also monitored and showed that even after the stimulated emission had reduced to zero there was still pumping of the 4p states. This is further evidence that the process must be a lower level effect which stops the stimulated emission oscillation.

It was possible to estimate the current density when the stimulated emission began to decrease and this value was about 2800 Acm^{-2}. This would indicate the point at which radiation trapping effects are becoming large enough to increase the lifetime of the lower level and destroy the population inversion. This value is of the same order as the value indicated in section 6.3 from the streak photography results.

7.6 Dependence of threshold on the current pulse risetime.

If the threshold current for laser action is plotted against the rate of rise of the current pulse (fig. 7.6) it is seen that there is a linear dependence with the correlation that short risetime gives a high current threshold. It is possible to find a theory to explain this for current densities below 2000 Acm^{-2}. We make the assumption that the direct pumping of the upper level is predominantly from the ion ground state which has a density N_i cm^{-3}. The rate equation for the

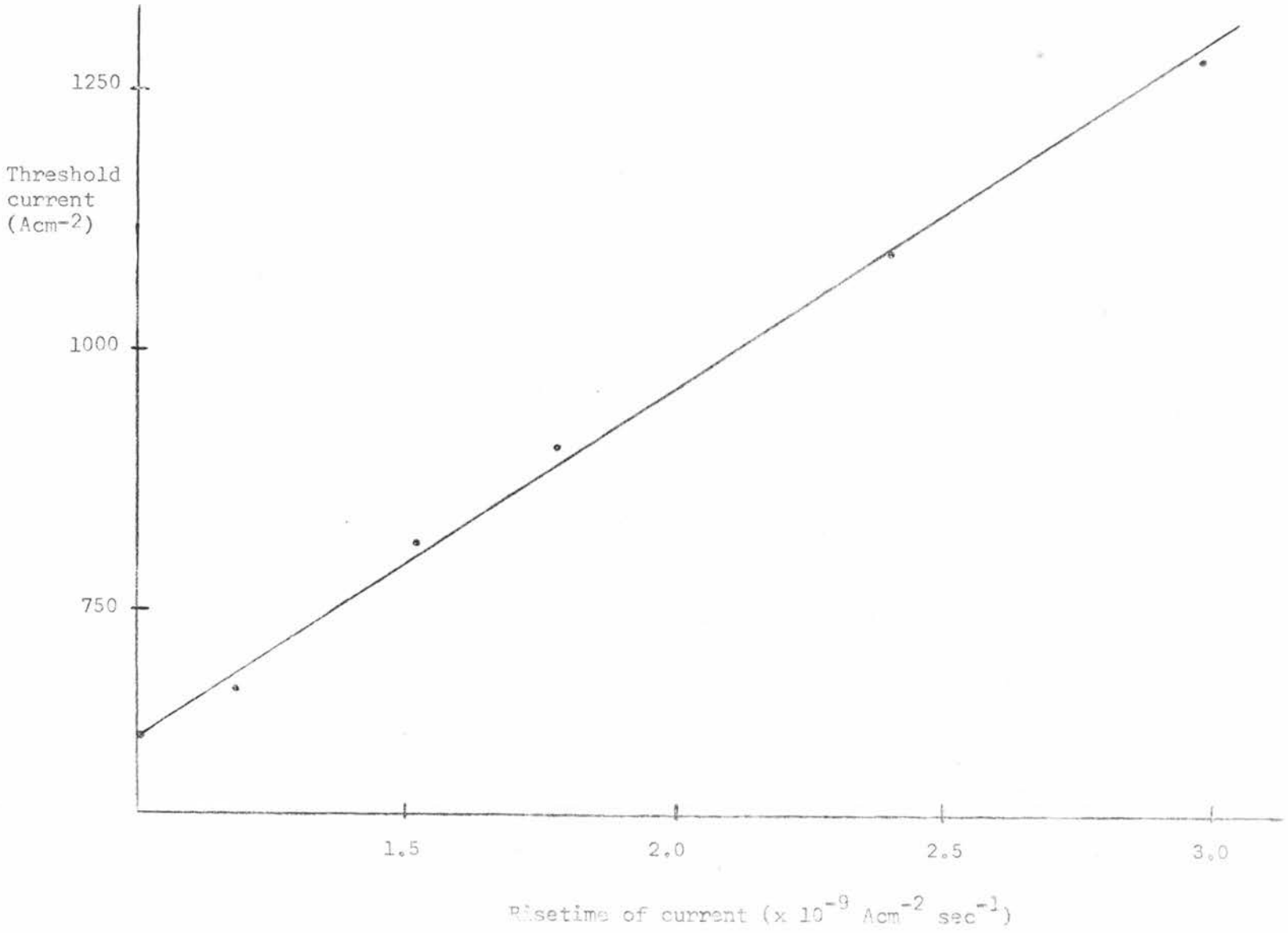

Fig. 7.6: Variation of threshold for stimulated emission with current rate of rise.

upper level can then be written

$$\frac{dN_1}{dt} = N_e N_i \langle \sigma v \rangle_{ei} - A_{12} N_1 - \bar{N} + \sum_K A_{K1} N_K \qquad (7.6.1)$$

where N_K = population density of state K where K = 1 represents upper laser level

N_e = electron density

$\langle \sigma v \rangle_{ei}$ = product of collision cross section for electron-ion collisions and electron velocity averaged over the velocity distribution.

A_{ij} = Einstein A coefficient for transition $i \rightarrow j$

$\bar{N}$ = number of stimulated photons cm^{-3} sec^{-1}.

From the results of Rudko and Tang (21) it can be shown that the cascade contribution $\sum_K A_{K1} N_K$ is an order of magnitude less than the spontaneous decay $A_{12} N_1$ so it is neglected. Also if the laser is at threshold neglect $\bar{N}$, giving equation (7.6.1) as

$$\frac{dN_1}{dt} = N_e N_i \langle \sigma v \rangle_{ei} - A_{12} N_1 \qquad (7.6.2)$$

It has been shown in section 7.1 that $N_1 = KI^2$ for low current densities so assuming $N_e = N_i$ and that the electron density is proportional to the current density (6) (i.e. $N_e = CI$) we have

in (7.6.2)

$$\frac{dI}{dt} = \left[\frac{C^2}{2K} \langle \sigma v \rangle_{ei} - \frac{A_{12}}{2} \right] I \qquad (7.6.3)$$

This linear behaviour explains fig. 7.6 and from this the gradient can be found. Substituting a value for A_{12} from the results of Rudko and Tang (21) gives

$$\frac{C^2}{2K} \langle \sigma v \rangle_{ei} = 2.61.10^{7} \text{ sec}^{-1} \qquad (7.6.4)$$

From the results of Sobolev et al (6) the constant C can be found to be $C = 5.10^{11}\ A^{-1}.cm^{-1}$. The constant K can be found from the results of Rudko and Tang (21) where $N_1 = 3.10^{9}\ cm^{-3}$ at a current density of about 170 Acm^{-2}, giving $K = 1.04.10^{5}\ A^{-2}.cm$. Substitution for C and K in equation (7.6.4) gives a value for $\langle \sigma v \rangle_{ei} = 2.2.10^{-11}\ cm^{3}\ sec^{-1}$. This is comparable with the calculated results of Sobolev et al (38) for the cross section for excitation from the 3p → 4p ion states. This means that it is reasonable to expect that the collisional de-excitation is in fact of sufficient magnitude to produce an effect on the population of the 4p states as was assumed from Sobolev's results in previous sections.

CHAPTER VIII - SUMMARY.

The present investigation carried out on a 4mm bore 3m long argon ion laser under pulsed conditions, with current densities between 1000 Acm^{-2} and 6000 Acm^{-2}, has shown that the populations of the ion levels have a varying dependence on the current density. In the region below 2000 Acm^{-2} there is a quadratic dependence of the spontaneous emission on current density, and, since the spontaneous emission intensity is directly dependent on the population in the upper level of the transition, the population depends quadratically on current density. This implies that the dominant excitation mechanism is of the multistep type, through an intermediate metastable state (section 4.3). Using a simple model of excitation from the Argon ion ground state by electron collision, in the region below 1500 Acm^{-2}, it was possible to explain the observed behaviour of the stimulated emission threshold with the current pulse risetime, and, by measurement, find a value for the collision cross section which agreed reasonably with the calculated values of Sobolev (section 7.6). A cross section of this order of magnitude would then imply that collisional de-excitation would be significant at about 3000 Acm^{-2}. This agrees with other results discussed below.

Between current densities of 2000 Acm^{-2} and 5000 Acm^{-2}, the populations of the upper levels begin to show a more linear dependence on the current density. There is evidence for two possible mechanisms occurring in this region. One is a single step excitation (section 4.2) which would give a linear relation between the populations and the current density. Evidence for this mechanism is found in section 6.2, where calculations show that the threshold for this mechanism agrees with the observed behaviour of the delays between the oscillating wavelengths. Another possible mechanism is deexcitation by electron collisions, or excitation from the 4s metastable states by electron collisions. This would also lead to a linear dependence of the populations in the ion states on current density (section 4.6). Further evidence for a mechanism of this type is shown in sections 7.3 and 7.4. It was shown in section 7.6 that this mechanism could be expected on the basis of the magnitude of the collision cross section.

Above a current density of 5000 Acm^{-2}, a complete saturation of the upper state populations is observed, and calculations in section 7.2 show that it is reasonable to explain this behaviour on the basis of depletion of the argon atom ground state population by collisions. The saturation of the upper laser levels coupled with a short lifetime caused by collisions

give favourable conditions for stimulated emission and the observed output increases more rapidly than would be expected from Lamb's theory (section 7.4).

Quenching of the stimulated emission was observed before the spontaneous emission has reached its peak, and this implies that some lower level effect is impeding the stimulation mechanism. This behaviour is interpreted in terms of a radiation trapping process on the lower levels for the transition. The observed initiation of this mechanism agrees favourably with work by Cheo and Cooper on radiation trapping (section 7.5).

The above work could be extended to more delicate measurements if some means could be found of reducing the noise inherent in the system. The discharge tube radiates noise during the pulse and produces considerable pick-up on the measuring apparatus. Care with screening and earthing minimises this effect, but it is still limiting. It would perhaps be possible then, to extend the measurements of section 7.6 to find the electron collision cross sections between the Argon ion states.

REFERENCES

(1) W.E. Bell (1964) Applied Phys. Letters 4, p.34.

(2) W.B. Bridges and A.N. Chester (1965) App. Opt. 4, p.573.

(3) R.A. McFarlane (1964) App. Opt. 3, p.1196.

(4) W.B. Bridges (1964) App. Phys. Letters 4, p.128.

(5) E.I. Gordon et al (1964) App. Phys. Letters 4, p.178.

(6) V.F. Kitaeva et al (1966) IE^3 J. of Quant. Elec. QE-2, no.9, p.635.

(7) E.C. Kemble (1937) Fundamental Principles of Quant. Mechs. (McGraw-Hill).

(8) W.V. Smith and P.P. Sorokin (1966) The Laser p.21 (McGraw-Hill).

(9) J.H. Van Vleck and V.F. Weisskopf (1945) Rev. Mod. Phys. 17, p.227.

(10) A.C.G. Mitchell and M.W. Zemansky (1961) Resonance Radiation and Excited Atoms (Cambridge Univ. Press).

(11) B.A. Lengyel (1966) Introduction to Laser Physics p.73 (Wiley and Sons).

(12) A.G. Fox and T. Li (1961) Bell Syst. Tech. J. 40, p.453.

(13) G.D. Boyd and J.P. Gordon (1961) Bell Syst. Tech. J. 40, p.489.

(14) A. Yariv (1967) Quantum Electronics, p.267 (Wiley and Sons).

(15) E.J. Gordon et al (1963) Optical Masers p.309 (Polytechnic Press).

(16) W.R. Bennett (1965) Appl. Opt. Suppl. 2 Chemical Lasers p.3.

(17) A.D. White and E.I. Gordon (1963) App. Phys. Letters 3, p.197.

(18) C.K. Patel (1964) Phys. Rev. Letters 12, p.588.

(19) L. Minnhagen (1963) Arkiv för Physik Band 25, no.19, p.203.

(20) W.R. Bennett et al (1964) App. Phys. Letters 5, no.8, p.158.

(21) R.I. Rudko and C.L. Tang (1967) J. of App. Phys. 38, no.12, p.4731.

(22) H. Statz et al (1966) Physics of Quantum Electronics p.674 (McGraw-Hill).

(23) H.N. Olsen (1963) J. of Quan. Spect. Radiative Transfer 3, p.59.

(24) W.R. Bennett et al (1962) Ann. Phys. 18, p.367.

(25) W.R. Bennett et al (1964) App. Phys. Letters 4, no.10, p.180.

(26) R.A. McFarlane (1964) App. Phys. Letters 5, no.5, p.91.

(27) R.A. McFarlane (1964) Phys. Rev. 133, A1476.

(28) S. Koozekanani(1966) IE^3 J. of Quant. Elec. QE-2, no.12.

(29) W. Lamb and Skinner (1950) Phys. Rev. 78, p.539.

(30) St. John and K. Lin (1964) J. of Chem. Phys. 41, p.195.

(31) W.R. Bennett (1966) Phys. Rev. Letters 17, no.19, p.987.

(32) L.A. Vainshtein and A.V. Vinogradov (1967) Zh.E.T.F. Pis'ma 5, no.9, p.328.

(33) L.A. Vainshtein and A.V. Vinogradov (1967) Optika y Spektrokopiya 23.

(34) S. Koozekanani (1967) App. Phys. Letters 11, no.3, p.107.

(35) E.I. Gordon and E.F. Labuda (1964) App. Phys. Letters 4, no.10, p.178.

(36) W.R. Bennett and W. Lichten (unpublished).

(37) E.I. Gordon et al (1966) Phys. of Quantum Electronics p.664 (McGraw-Hill).

(38) I.L. Beigman et al (1967) Zh. E.T.F. Pis'ma 6, no.10, p.919.

(39) K.T. Compton (1922) Phys. Rev. 20, p.283.

(40) T. Holstein (1947) Phys. Rev. 72, no.12, p.1212.

(41) M. Zemansky (1927) Phys. Rev. 29, p.513.

(42) W.R. Bennett (1965) App. Opt. Suppl. on Chemical Lasers p.8.

(43) W.R. Bennett (1962) App. Opt. Suppl. 1, p.24.

(44) A.L. Bloom et al (1964) Phys. Rev. 135, A578.

(45) P.K. Cheo and H.G. Cooper (1965) App. Phys. Letters 6, no.9, p.177.

(46) A. Klein (1968) Paper presented at Quantum Electronics conference in Miami.

(47) W.R. Bennett et al (1964) App. Phys. Letters 5, no.8, p.158.

(48) V.F. Kitaeva et al (1966) Zh.E.T.F. Pis'ma 4, no.6, p.146.

(49) R.H. Neusel (1966) IE^3 J. of Quant. Elec. 2, p.331.

(50) C.G.B. Garrett (1967) Gas Lasers p.18 (McGraw-Hill).

(51) W.W. Rigrod (1965) J. of App. Phys. 36, no.8, p.2487.

(52) W.E. Lamb (1964) Phys. Rev. 134, A1429.

Acknowledgements

I should like to record my appreciation to friends and colleagues for the help given to me. I am particularly grateful for the advice from and discussions with my supervisor Mr. A. Maitland and my colleagues Dr. A. Smith and Mr. M.H. Dunn. Construction of the laser would have been impossible without the help of the glassblower Mr. F. Akerboom and in many experiments the assistance of my wife was invaluable. Thanks is due also to Mr. J. Spark for the preparation of the photographs, to Mr. T. McQueen for the copying of the thesis, to Mrs. C. MacArthur for the typing of the thesis, and to the workshop staff for the construction of specialised equipment. My thanks is also due to the Carnegie Trust for Scotland who provided a grant for this work, and to the Caird Trust and the University of St. Andrews for grants enabling me to attend the Conference on Quantum Electronics in Miami.